Avalonia Get Bent! Paleomagnetism from SW Iberia confirms the Greater Cantabrian Orocline

This paper is a preprint.

It will be submitted to Geosciences Frontiers during the first week FEBRUARY 2020

Bruno Daniel Leite-Mendes[1], *Daniel Pastor-Galán[2,3,4], Mark J. Dekkers[1], Wout Krijgsman[1]

[1]Paleomagnetic Laboratory, Fort Hoofddijk, Department of Earth Sciences, Utrecht University, Budapestlaan 17, 3584CD, The Netherlands

[2]Frontier Research Institute for Interdisciplinary Sciences, Tohoku University, Japan

[3]Department Earth Science, Tohoku University, Japan

[4]Center for North East Asia Studies, Tohoku University, 980-8576, 41 Kawauchi, Aoba-ku, Sendai, Miyagi, Japan.

*Corresponding author: pastor.galan.daniel.a8@tohoku.ac.jp

Avalonia, get bent!
Paleomagnetism from SW Iberia confirms the Greater Cantabrian Orocline

Bruno Daniel Leite-Mendes[1], Daniel Pastor-Galán[2,3,4], Mark J. Dekkers[1], Wout Krijgsman[1]

[1]Paleomagnetic Laboratory, Fort Hoofddijk, Department of Earth Sciences, Utrecht University, Budapestlaan 17, 3584CD, The Netherlands

[2]Frontier Research Institute for Interdisciplinary Sciences, Tohoku University, Japan

[3]Department Earth Science, Tohoku University, Japan

[4]Center for North East Asia Studies, Tohoku University, 980-8576, 41 Kawauchi, Aoba-ku, Sendai, Miyagi, Japan.

Abstract

The amalgamation of Pangea formed the contorted Variscan-Alleghanian orogen, suturing Gondwana and Laurussia during the Carboniferous. From all swirls of this orogen, a double curve stands out in Iberia, the coupled Cantabrian Orocline and Central Iberian Curve. The Cantabrian Orocline formed subsequent to Variscan orogeny (ca. 315-295 Ma). The mechanisms of formation for this orocline are disputed, with an Avalonian (Laurussia) indenter of south-westernmost Iberia; and a change in the stress field that buckled the orogen, as the most prominent. In contrast, the geometry and kinematics of the Central Iberian curve are largely unknown. Whereas some authors defend both curvatures are genetically linked, others support they are distinct and formed at different times. Such uncertainty adds an extra layer of complexity into our understanding of the final stages of Pangea formation. To solve these issues, we study the late Carboniferous kinematics of SW Iberia with paleomagnetism. Our results show up to 70˚counterclockwise vertical axis rotations at late Carboniferous, coincident with the kinematics expected in the southern limb of the Cantabrian Orocline. These results discard a concomitant formation of both Cantabrian and Central Iberian curvature. The coherent rotation of both Gonwdanan and

Avalonian pieces of SW Iberia confirms the Greater Cantabrian Orocline hypothesis and discards the Avalonian indenter as a mechanism of formation for the Cantabrian Orocline. The Greater Cantabrian Orocline extended beyond the Rheic Ocean suture affecting both Laurussia and Gondwana margins and probably formed due to a late Carboniferous change in the stress field.

Keywords: Pangea, Variscan orogeny, Greater Cantabrian Orocline, Paleomagnetism, Central Iberian Curve

Highlights:

-Paleomagnetism indicates that SW Iberia rotated ~70˚CCW during late Carboniferous

-The rotation is coeval and of the same magnitude to the Cantabrian Orocline

-The Central Iberian curvature had to form before, probably at early Carboniferous

-Indentation cannot explain the curvature and kinematics of the Cantabrian Orocline

-We confirm the Greater Cantabrian Orocline that affected Gondwana and Laurussia

1 Introduction

Most orogens show certain degree of curvature when observed in plan-view. These curves can range from minor deflections of orogen trend at a thrust scale (Izquierdo-Llavall et al., 2018) to bends affecting the entire lithosphere (Li et al., 2012). The mechanisms that form curved mountain belts like irregular collisions, changes in stress field, basin architecture; terrain wrecks, etc., are extremely varied (Marshak, 2004; Johnston et al., 2013). Therefore, and despite being widespread around the globe, curved mountain belts' kinematics and their geodynamic consequences remain mysterious and fascinating.

The Paleozoic era is dominated by the amalgamation of Pangea (e.g. Torsvik and Cocks, 2017), the latest continental superplate (Pastor-Galán et al. 2019). One of the Pangea-forming collisions, between Gondwana and Laurussia, (e.g. Stampfli and Borel, 2002; Stampfli, 2013; Domeier and Torsvik, 2014) formed the long and winding Carboniferous Variscan-Alleghanian orogen (Fig. 1). This contorted orogen has in Iberia its most prominent curves: the Cantabrian Orocline, to the north, and a Central Iberian Curve, to the south (Fig.1 and 2a). The Cantabrian Orocline draws a nearly 180º curvature running from Brittany (present day France), through the Bay of Biscay, into central Iberia. This orocline formed after the main Variscan deformation phases (310-295 Ma; e.g. Weil et al., 2019).

In contrast, the geometry and kinematics of the Central Iberian Curve are still under debate (e.g. Weil et al., 2019) (Fig. 1 and 2a). Largely due to the lack of constraints, the proposed mechanisms for the formation of both structures are contradictory. Some authors consider these two structures formed coevally as a coupled-orocline (e.g. Martínez Catalán 2011; Shaw et al., 2012). Other studies suggest that any vertical axis rotations in the Central Iberian Curve have to predate the formation of the Cantabrian Orocline (Pastor-Galán et al., 2016; Jacques et al., 2018a; Azor et al., 2019). Mechanisms suggested that are capable to explain the available data include: 1) A mid-to-late Carboniferous indentation of Laurussia into Gondwana at SW Iberia (Fig. 3) (e.g. Lorentz, 1976; Simancas et al. 2013); and 2) a post-Variscan change in the stress field due to plate reorganizations after Pangea amalgamation (e.g. Martinez-Catalan 2011; Gutierrez-Alonso et al., 2008a; Pastor-Galán et al., 2015b). Following this second scenario, Pastor-Galán et al. (2015a) hypothesized the

Greater Cantabrian Orocline that would have bent around a vertical axis the entire Variscan orogen, including a previously formed Central Iberian curve. This structure would trespass the main lithospheric scale structures and sutures, affecting both Gondwana and Laurussia margins.

In this paper, we investigate the kinematics of Iberia during the Late Carboniferous through paleomagnetic analyses in SW Iberia, which lacks such data (Fig. 2a). Paleomagnetism is the best tool available to study vertical axis rotations due to the independence of the Earth's magnetic field to the orogen structures (e.g. van der Boon et al., 2018; Rezaeian et al., in press). Paleomagnetism from SW Iberia is crucial to clarify (1) the relationship between both Cantabrian and Central Iberian curves, (2) the mechanism of formation of those orogenic curves and (3) their role within the frame of Pangea amalgamation. Our results show general ~70º counterclockwise (CCW) rotations in southwestern Iberia, coeval and of the same magnitude to the expected in the southern limb of the Cantabrian Orocline. Such rotations, rule out both a late Carboniferous indenter in SW Iberia and a coeval formation of both Cantabrian and Central Iberian curvature. Our results confirm the Greater Cantabrian Orocline hypothesis, which buckled both continental margins of Gondwana and Laurussia at the latest stages of the formation of Pangea.

2 Geological Setting

The Silurian collisions between Laurentia, Baltica and Avalonia (s.l.) formed Laurussia (e.g. Mac Niocaill et al., 2000; Domeier, 2016). From late Devonian, Laurussia, Gondwana, Siberia and some minor plates amalgamated into the supercontinent Pangea (e.g. Nance et al., 2010). One of the most striking relics of the formation of Pangea is the Variscan-Alleghanian orogen, the result of the final collision between Gondwana and Laurussia, which extends from Europe and northeast Africa to southern North America (Fig. 1). The collision began at late Devonian in eastern Europe and youngs westwards towards south North America, where it commenced at late ~325 Ma, coeval with the collapse of the European sector (e.g. Faure et al., 2009; Hatcher, 2010). . This belt shows a variable trend with a succession of orogenic curves of all types (Fig. 1): The Bohemian curve (e.g. Tait et al., 1996), the coupled Cantabrian Orocline (e.g. Gutierrez-Alonso et al., 2012) and Central

Iberian curve (e.g. Aerden, 2004), the Atlantic Canada (e.g. O'Brien, 2012), Pennsylvanian and Alabama curves (e.g. Thomas, 1977).

2.1 The Variscan belt in SW Iberia

The Iberian massif contains an almost continuous cross section of the Variscan orogen (e.g. Lotze 1945, Julivert 1974, Ribeiro et al. 2007) (Fig. 2a). Geographically, the external zones of the Gondwana margin are nestled at the core of the Cantabrian Orocline, to the north, and the hinterland zones are to the west and center (Fig. 2a; e.g. Díaz Balda, 1995; Azor et al., 2019). Southwest Iberia hosts also a piece of the hinterland with a sector of the Central Iberian and Ossa Morena zones (Fig. 2b). Finally, southwestern-most Iberia contains a putative suture of the Rheic ocean, and a piece of the Laurussian margin fold-and thrust belt, the South Portuguese Zone (e.g. Oliveira et al., 2019a) (Fig. 2a).

The orogen in Iberia shows multiple deformation, metamorphic and magmatic events (e.g. Martínez-Catalán et al., 2014; Azor et al., 2019): (1) An initial continent-continent collision began ca. 370-365 Ma together with high pressure metamorphism (e.g. Lopez-Carmona et al. 2014). (2) Between 360 and 330 Ma multiphase shortening phase (frequently referred to as D1), accompanied by barrovian type metamorphism (e.g. Dias da Silva et al., in press) and plutonism at ~340 Ma (e.g. Gutiérrez-Alonso et al., 2018). (3) An extensional collapse, so-called D2, at ~330-318 Ma, which formed core-complexes and granitic domes (e.g. Rubio Pascual et al. 2013; López-Moro et al., 2018). This event is coeval and genetically linked to the formation of a foreland fold-and-thrust-belt (e.g. Pastor-Galán et al., 2009). Lastly (4) a final shortening event (D3) occurred ca. 315-290 Ma, associated to the formation of the Cantabrian Orocline and accompanied by the general intrusion of mantle derived granitoids (e.g. Pastor-Galán et al., 2012a).

In SW Iberia, the aforementioned events are characterized by a sinistral component of deformation, which contrasts with the general dextral component recognized in most regions of the orogen (e.g. Martínez Catalán et al., 2011; Gutiérrez-Alonso et al., 2016). Late Devonian collisional structures (D1) formed NE-vergent recumbent folds in the southernmost Central Iberian Zone and SW-vergent folds and thrusts in Ossa Morena and

South Portuguese zones. This phase continued with an early Carboniferous transtensional event that extended variably the continental lithosphere (e.g. Pérez-Cáceres et al. 2015), developed deep basins and widespread sinistral shearing (e.g. Azor et al., 2019). Coevally an important extension-related magmatic event happened, perhaps assisted by a plume-type mantle (Simancas et al. 2006) or a slab break-off (Pin et al. 2008). After this event, a left-lateral transpressional event happened forming the shear bands to the north and south of Ossa Morena Zone (Fig. 2b), which accommodated the majority of the transcurrency. However, left-lateral displacements are observable all along Ossa Morena and South Portuguese Zones. Pérez-Cáceres et al. (2016) estimated over 1000 km of collisional convergence in SW Iberia, most of them corresponding to left-lateral displacements parallel to terrane boundaries.

The South Potuguese Zone constitutes the Laurussian foreland fold-and-thrust belt in the Iberian variscices (e.g. Pérez-Cáceres et al., 2017). Its three units are the Pulo de Lobo, Iberian Pyrite Belt and the Baixo Alentejo Flysch. Pulo de Lobo unit is a low metamorphic grade accretionary prism with clastic sedimentary rocks and basalts with MORB signature, formed ~380-370 Ma and indicating a (Rheic?) suture (e.g. Azor et al., 2019). The Iberian Pyrite Belt is world class volcanogenic massive sulfide deposit and consists of three formations: Phyllite and Quartzite formation (~390 to ~360 Ma); the Volcano-Sedimentary Complex (~360 to ~330 Ma); and the Culm turbiditic sequence of ~330 Ma of age (e.g. Oliveira et al., 2019a). The Volcano-Sedimentary complex shows alternation of bi-modal volcanic rocks and sedimentary levels (e.g. Oliveira et al., 2019a; 2019b). Overlaying it, the Baixo Alentejo Flysch at the southwest is a composite turbiditic sequence spanning from ~330 to ~310 Ma (Oliveira et al., 2019b). The South Portuguese Zone has a curved trend that roughly follows the Cantabrian Orocline with a varying strike from 160˚(NW) to roughly 90˚(E) (Fig. 2b). The zone shows no or low internal deformation and metamorphism, which increases northwards, towards the suture (Onezime et al., 2002; Pérez-Cáceres et al., 2016; Azor et al., 2019).

The boundary between the South Portuguese and Ossa Morena zones is a sinistral shear zone (Beja-Acebuches) that contains a strongly deformed amphibolitic belt with oceanic affinity (Munha et al. 1986, 1989; Quesada et al., 2019). This belt possibly represents relics

of the Rheic ocean, or a subsidiary seaway opened during transtension (e.g. Pérez-Cáceres et al., 2015; Quesada et al., 2019). To the west, the limit is marked by a series of igneous rocks including the early Carboniferous Toca de Moura basaltic complex (Gonçalves 1985, Santos et al. 1987, Santos et al.1990).

The Ossa-Morena Zone lies to the north of the suture, and is a distal platform of Gondwana (e.g. Arenas et al., 2016). It comprises an Ediacaran continental arc and Lower Paleozoic volcanic and sedimentary sequences (Eguiluz, 1987; Quesada, 1996, Sánchez-García et al., 2019). The Ediacaran arc contains volcanic, plutonic and shallow marine sedimentary rocks (e.g. Eguiluz 1987). Overlying the Ediacaran arc, a rift-to-drift Cambrian to Middle Ordovician sequence crops out with early Cambrian rift magmatism, iron-rich carbonates and volcano-sedimentary rocks (Liñan and Quesada, 1990; Sánchez-García and Quesada, 2001). Conformably over the rift-to-drift sequence, a ~7000 m series of mid-Ordovician to mid-Devonian passive margin siliciclastics with Gondwana affinity occur (Robardet and Dore 1988; Gutiérrez-Marco et al., 2019), followed by syn-orogenic turbidites (Sánchez-Garcia, 2003). Structurally, Ossa Morena behaves as a large-scale sinistral strike-slip duplex, formed during the early stages of the orogeny, and reactivated in later stages (e.g. Quesada & Dallmeyer 1994). During the Variscan orogeny, Ossa Morena underwent greenschists metamorphism.

The Central Iberian Zone is the largest in the Variscan Iberia and extends from northwesternmost of Iberia to the southwestern sector. In the SW, the contact between this zone and Ossa Morena is a sinistral shear zone (Badajoz-Cordoba) (Fig. 2a). Its stratigraphy starts with an Ediacaran to early Cambrian forearc turbiditic sequence, overlain by a passive margin Paleozoic sequence, spanning from Cambrian to Devonian times (Valladares, 2000). There are occurrences of Siluro-Devonian volcanic rocks (e.g. Gutiérrez-Alonso et al., 2008b), remarkably at the Almadén syncline, near its boundary with Ossa Morena. During the Variscan orogeny, the Central Iberian Zone underwent the formerly described D1, D2 and D3 deformation phases and Barrovian metamorphism (e.g. Díaz-Balda et al, 1995; Dias da Silva et al., in press).

2.2 Curvature in the Iberian variscides

The kinematic classification of orogen curvature distinguishes two end members (Weil and Susmann, 2004; Weil and Yonkee, 2009; Johnston et al., 2013; Pastor-Galán et al., 2017a): 1) Primary arcs, orogenic curves in plan view that pre-existed the main orogenic event, for example an embayment; 2) Secondary oroclines, are orogenic bends whose whole curvature is the product of bending/buckling the originally linear main orogen around a vertical axis (e.g. Eldrege et al., 1985). Progressive oroclines are all the orogenic curves whose curvature is only partially due to vertical axis rotations (e.g. Meijers et al., 2017).

The Cantabrian Orocline starts in Brittany and follows a near 180º change in strike through the Bay of Biscay, into the NW Iberian peninsula. There, it apparently turns back with an opposite sense curvature known as the Central Iberian curve (Figs. 1 and 2a). The Cantabrian Orocline is one of the most studied oroclines in the world (e.g. Weil et al., 2013; Murphy et al., 2016). Its curved geometry and structural style are well studied (e.g. Julivert and Marcos, 1973; Gutiérrez-Alonso 1996; Merino-Tomé et al., 2009; Pastor-Galán et al., 2012b, Shaw et al., 2016). Kinematically it has been constrained as a secondary orocline after extensive paleomagnetism (e.g. Hirt et al., 1993; Weil et al., 2000), structural geology (e.g. Kollmeier et al., 2001; Pastor-Galán et al., 2014) and geochronology (e.g. Gutiérrez-Alonso et al., 2011; 2015). The Cantabrian Orocline buckled a linear portion of the Variscan orogen around a vertical axis in a short period of time between 315 to 290 Ma, during D3 (e.g. Pastor-Galán et al., 2011; Fernández-Lozano et al., 2019). Paleomagnetic data from Ireland (Pastor-Galán et al., 2015a) show coeval clockwise rotations of similar magnitude as in the northern limb of the Cantabrian Orocline supporting the Greater Cantabrian Orocline hypothesis, in which the orocline formation would affect both Gondwana and Laurussia margins.

In contrast, the geometry and kinematics of the curvature to the South, the Central Iberian curve (e.g. Staub, 1927; Aerden, 2004; Figs. 1 and 2) are poorly known. This curve's geometry is under debate with three competing proposals (Aerden, 2004; Martínez Catalán, 2012: Shaw et al., 2012). The curvature is most obvious at the boundary between Galicia-Tras os Montes and Central Iberian Zones and to the SE of the Central Iberian Zone (Fig. 2a; Martínez-Catalán, 2012). Previously, most authors considered the >20˚change in strike of the Iberian ranges (NE Iberia, Fig. 2a) part of the Central Iberian curve's hinge (e.g.

Shaw et al., 2012), but recent studies proved a Cenozoic origin for such deflection (Calvín et al., 2014; Pastor-Galán et al., 2018; Izquierdo-Llavall et al., 2018). The available late Carboniferous kinematic data from central Iberia do not allow for a coeval formation of both curvatures (e.g. Pastor-Galán et al., 2015b, Jaques et al., 2018a)(Fig. 2a). Late Carboniferous paleomagnetic data show no differential rotations between the limbs of the Central Iberian curve and general CCW rotations, compatible with the Cantabrian Orocline formation (e.g. Pastor-Galán et al., 2016) (Fig. 2a). Structurally, D3 deformation patterns around the Galicia-tras-Os-Montes Zone do not support differential vertical axis rotations during the late Carboniferous (Dias et al., 2016; Jacques et al., 2018b; Pastor-Galán et al., 2019; Dias da Silva, in press). Together, all these data-sets only allow a pre-320 Ma formation for the Central Iberian curve.

A plethora of mechanisms have been suggested to explain the formation of the Cantabrian Orocline (e.g. Weil et al., 2013; 2019). The only mechanisms proposed so far that can explain the secondary nature of the Cantabrian Orocline and perhaps the Central Iberian curvature are: (1) the indentation of Laurussia in SW Iberia (e.g. Lorenz et al., 1984; Simancas et al., 2005) (Fig. 3a) and (2) a change in the stress field during the late Carboniferous (e.g. Ries and Shackleton, 1976; Gutiérrez-Alonso et al., 2004) (Fig. 3b). The indenter model suggests that a promontory with Avalonian affinity, the South Portuguese Zone (Pérez-Cáceres et al., 2017), collided into Gondwana during the Carboniferous (Fig. 3a). The indenter would nucleate first the Central Iberian curve and later the Cantabrian Orocline (Simancas et al., 2013). The stress-change model, explains that at the late Carboniferous the stress field flipped from orogen perpendicular shortening to orogen parallel (e.g. Merino-Tomé et al., 2009; Murphy et al., 2016; Fig. 3b). Mechanisms suggested that could produce such change include a diachronic closure of the Rheic ocean (Pastor-Galán et al., 2015b), self-subduction of Pangea in the Paleotethyan realm (Gutiérrez-Alonso et al., 2008a), a Pangea B to Pangea A transition mega-shear (Martínez-García, 2013; Martínez-Catalán, 2011) or subduction roll-back of the Paleotethys (Pereira et al., 2015).

2.3 Previous paleomagnetism in SW Iberia

The only previous paleomagnetic study including the Ossa Morena and South Portuguese zones focused on the Beja Gabbroic Massif, Portugal (Perroud et al. 1985). Data shows varied inclinations and declinations in the gabbros and complex overprints elsewhere. The authors did not consider any structural corrections, assuming the gabbro was undeformed. Recently, Dias da Silva et al. (2018) showed that the area underwent strong deformation during the Carboniferous. The dataset is untrustable without knowing which corrections should be applied.

Paleomagnetic data from the northern and central sectors of the Central Iberian Zone show a widespread late Carboniferous remagnetization in sedimentary rocks, a primary magnetization in D2 granites (intruded ~320 Ma), and significant CCW rotations (Pastor-Galán et al., 2015b; 2016; 2017b; Fernández-Lozano et al., 2016) (Fig. 2a). Two previous studies identified a possibly different magnetization at Almadén syncline region, SE Central Iberian Zone (Perroud et al., 1991; Pares & Van der Voo, 1992) (Fig. 2a; 2c).

The Almadén syncline is a 30 km long and 15 km wide with ~100˚ trend structure (e.g Aller et al.,1986) (Fig. 2c). Its fold axis is horizontal through most of the structure, but becomes steeply plunging and conical in shape at its eastern periclinal closure (Vergés, 1983). The structure formed during D1 (Vergés, 1983) and underwent left-lateral transcurrency at D3 (Aller et al., 1986). This D3 transcurrency formed fragile-ductile shear bands and locally a rough cleavage (Aller et al., 1986; Palero-Fernández et al., 2014). A large amount of volcanic rocks are intercalated between the marine strata in its Silurian-Devonian stratigraphy, and hosts the largest concentration of mercury in the world (Palero-Fernandez et al. 2014). Both previous paleomagnetic studies in Almadén, by Perroud et al. (1991, Silurian Tuffs and Lavas) and Parés and van der Voo (1992; Ordovician flows and Devonian dolerites), identified two different magnetization components. The first component, so-called "I" or "B" (Perroud et al., 1991; Parés and van der Voo, 1992 respectively), is downwards, single polarity and shallow with declinations towards the E or SE, which demagnetizes up to 500˚ C and 40 mT (Supplementary File SF1-C). Both studies conclude this component is a late Carboniferous overprint with CCW rotations coeval with the formation of the Cantabrian Orocline (Pastor-Galán et al., 2015b).

The second component, "II" or "C" (Perroud et al., 1991; Parés et al., 1992 respectively), is also single polarity component, but points upwards with inclinations ca. -35˚ and declinations to the NE. This is a high temperature and coercivity component (400ºC to 600ºC and 40-100mT). Perroud et al. (1991) interpreted "II" as Silurian, since k (precision parameter) got slightly higher after a correction for eastern syncline's distinctly plunging axes. We are cautious about the procedure since they applied a unique axial plunge correction to all sites, even to those where the axis does not plunge whatsoever. In addition, the structural data of Almadén syncline do not allow for reconstructing the actual movement of the axis to its present-day plunge. Uncertain corrections in conical or plunging axis usually result into spurious rotations making paleomagnetic directions difficult to interpret (Pueyo, 2003; Pueyo et al., 2016). In addition, Parés and van der Voo (1992) found the same component in Devonian dolerites before applying any correction and hypothesize an early Carboniferous origin. The meaning of "II" or "C" component remains puzzling, although if acquired during a normal polarity chron (declination ~ 250º), it would indicate about 90˚ CW rotation at SW Iberia, supporting a pre-320 Ma vertical axis rotation origin for the Central Iberian curve (Fig. 2a).

3 Methods and Results

We collected 429 oriented standard cylindrical core samples (diameter = 2.5 cm) with a petrol-powered drill in SW Iberia. We targeted 15 sites with fresh outcrops, non-metamorphic and with little to no internal deformation. We retrieved a minimum of 10 samples (3 sites) and preferably >20 (11 sites), one site resulted too hard to drill and collected only 4 cores (BD02) (Fig. 2a).

We labeled as BD the sites from the volcano-sedimentary complex of the South Portugese zone, and refer to this collection of samples as BD series. We sampled 8 sites (223 cores) in basic lavas and acidic tuffs (BD01, BD03, BD04, BD06-BD08), subvolcanic bodies (BD5), and Jaspers (BD02) along the orogen trend (Fig. 2b). JaIb series are all sites sampled in Ossa Morena Zone, where we recovered 114 cores at 5 different sites in Cambrian rocks near the limit with the South Portuguese Zone. We sampled Rheic ocean rift related volcanics (JaIb01-02), iron-rich limestones (JaIb04-05) and a Gabbroic intrusion, Cambrian

age (e.g. Cambeses et al., 2019)(Fig. 2b). Samples collected at Almadén Syncline constitute the QM series. We cored 90 samples at two sites: QM01 (31 cores), a Devonian dolerite at the core of the syncline which corresponds to the site AD01 from Pares and Van der Voo (1991); and QM02 (59 cores), Silurian tuffs and lavas previously sampled by Perroud et al. (1990, samples AM, AN, AO, AX and AY) (Fig. 2c). QM01 and QM02 correspond with the hinge and southern limb of Almadén syncline in an area with horizontal axis and no major structural complications (Fig 2c).

We performed rock magnetic (Fig. 4), AMS (Fig. 5) and paleomagnetic directional analyses (Fig. 6-10) to the sample collection at Paleomagnetic Laboratory 'Fort Hoofddijk', Utrecht University. Supplementary file SF1A contains a detailed outcrop description and Supplementary file SF2 the location. We also provide all rock magnetic data in the supplementary files SF3 and SF4, and paleomagnetic data and interpretation in SF5 and SF6 files (.col and .pub files from paleomagnetism.org, ; Koymans et al., in press), which are accessible through the persistent identifier [WRITE NUMBER HERE ONCE IT IS SET] of paleomagnetism.org.

3.1 Rock Magnetism

Thermomagnetic and micromagnetic analyses are useful to identify and understand the magnetic mineralogy and its magnetic history, as well as to select the best strategies for their stepwise demagnetization. We analyzed 19 samples, representative of our various lithologies. Thermomagnetic runs were performed with a modified horizontal translation Curie balance (Mullender et al. 1993) (Fig. 4; Supplementary File SF3A).

Many samples from BD series (South Portuguese Zone) show a paramagnetic curve with a drop in the magnetization between 500ºC and 560ºC, which evidences the presence of (Ti-)magnetite with a variable degree of Titanium substitution. BD01-35 (Fig. 4) shows a sharp drop between 660º and 680º C typical of hematite. BD02 (Sedimentary jasper, Fig.4) and BD06-12 (acidic tuffs) show a marked decrease of magnetization from 200° C to 400° C, and a later sharp decrease between 560°C and 580°C. BD06-5 shows a typical paramagnetic

curve with alteration at about 400-420º C indicating the presence of non magnetic sulfides (likely pyrite)(Supplementary File SF1-B).

JaIb series (Ossa Morena, Supplementary File SF1-B) show distinct magnetic behaviors. JaIb01 (red pillow lavas) shows a stable magnetization until 625°C followed by a sharp decrease up to 700° C, typical for hematite (Fig. 4). Curves of JaIb2 (spilite) and JaIb3 (gabbro, Fig. 4) show slight decay up to 560° C followed by a sharp decrease until 580°C, a classical behavior for magnetite. JaIb4 and JaIb5 (limestones) show a paramagnetic with sulfide alteration over 400℃, likely pyrite, and a minor decay at ~580° C, indicating some magnetite. A second sample of JaIb05 also shows a curve similar to that of greigite (Fig. 4) (Dekkers et al., 2000).

In QM series (Almadén, Supplementary File SF1-B), both QM01 (dolerite) and QM02 (lavas and tuffs) show a paramagnetic curve. QM01 (Fig.4), shows alteration over 400 ºC indicating the presence of non-magnetic sulfides (e.g. pyrite).

We obtained hysteresis loops with a Micromag AGFM 2900-02 apparatus (Fig. 4, Supplemental file SF3-B). The majority of the results of the micromagnetic analyses show a pseudo-single domain behavior (e.g. Fig. 4, BD02). BD01-35 (Fig.4) denotes hematite composition, which is coherent with the thermomagnetic analysis of this sample. Some sites (e.g. JaIb3 in Fig. 4) further show a nearly super-paramagnetic behavior. Some samples show an atypical behavior, which we consider to be failed measurements (e.g. Fig. 4, QM01).

3.2 Anisotropy of the magnetic susceptibility (AMS)

AMS is a very sensitive, non-destructive method to describe preferred orientations of mineral crystal axes, even in weakly deformed contexts (e.g., Borradaile, 2004; Pares, 2015). The AMS ellipsoid (k_{max}, long axis; k_{int}, intermediate axis; and k_{min}, short axis; Fig. 5) may work as a proxy for a deformation ellipse of a sample (Borradaile, 2004). We analysed a total of 169 samples with an AGICO MFK1-FA kappabridge (lowest detectable susceptibility change of 1x10-7 SI). We provide all AMS data files in Supplementary File SF4.

In BD series (South Portuguese), we analyzed sites BD01, 03, 04, 07 and 08 (Fig. 5). They show a magnetic susceptibility of ~10^{-4} SI and P ratios (k_{max}/k_{min}) below 1.12 (i.e. 12% anisotropy). All sites indicated a general tendency to oblate shape with the exception of BD04, which shows a quasi random fabric. Sites BD01 and BD03 show k_{int} and k_{min} elongated towards each other and perpendicular to the bedding plane (Fig 5). In sites BD07 and BD08, k_{max} and k_{min} elongate towards each other, along a non-bedding plane (Fig. 5).

We analysed all samples from JaIb series (Ossa Morena). JaIb1 (susceptibility 10^-4 SI, P = 1.3) and JaIb2 (~10^-3 SI, P = 1.14) show an oblate ellipsoid, in the case of JaIb1 with k_{min} perpendicular to the bedding plane (Fig 5). JaIb3 (gabbro) does not present a clear grouping of the anisotropy axes. JaIb4 (limestone) shows oblate ellipsoids but with a low anisotropy level with its short axis perpendicular to bedding (Fig. 5). Site JaIb5 results are varied with both oblate and prolate results and P values around 1.1. k_{max} coincides with the measured fold axis, k_{min} approximately coincides with the pole to bedding although it follows a follow a great circle with k_{int}, perpendicular to the fold axis.

From QM series, QM01 (dolerite) shows low anisotropy in all samples (susceptibility 10^-4 SI; $P<1.012$) and oblate shape. The tuffs and lavas of QM02 show slightly higher anisotropy (susceptibility varies from 10^{-4} to 10^{-3}; $1.02<P<1.1$) with k_{min} is loosely clustered, but unparallel to the bedding pole. k_{max} and k_{int} are, similarly to QM01, dispersed indistinguishable in a great circle.

3.3 Paleomagnetism

We obtained paleomagnetic directions with two 2G-SQUID cryogenic magnetometers for both alternating field (AF) and thermal demagnetization methods (Tauxe, 2010). Thermal demagnetization was performed in 20-50°C steps from room temperature to complete demagnetization (Fig. 6). AF demagnetization was performed with a robotized magnetometer (Mullender et al., 2016) with variable field increments (4-10 mT) up to 100 mT. We pre-heated our limestone samples up to 150°C prior to AF demagnetization to remove the effect of high-coercivity but low-blocking temperature minerals that may add errors (van Velzen & Zijderveld, 1995). Principal component analysis (Kirschvink, 1980)

was used to calculate magnetic component directions from "Zijderveld" diagrams (Zjiderveld, 1967) using Paleomagnetism.org (Koymans et al., 2016; Koymans et al., in press) (Fig. 6). We applied a fixed 45º cut-off to the VGP distributions of each site and used the Deenen et al. (2011) criteria to evaluate the scatter of VGPs (Fig. 8-10). In samples where the components are not fully resolved but follow a great circle path, we fitted a great circled instead. In such sites, we first identified any reliable component to subsequently fit great circle solutions (Fig. 6) following McFadden and McElhinny (1988) approach, combining great circles and linear best fits (Figs. 6-10). We provide a summary of the statistical parameters in table 1.

We analyzed the very low temperature/coercivity overprints in all sites and areas to scrutinize their origin. In most sites (only exceptions JaIb1, JaIb4 and JaIb5), this low temperature (20-200˚C) and low coercivity (0-16 mT) overprint is equal to the present-day field, and we named that component PD (Supplementary file SF1C).

A recurring component occurs in 7 sites through BD and JaIb series. This component shows a reversed single polarity with very shallow inclinations and declinations towards the SSE. It clusters better before any tilt correction (dec/inc =160.6°/1.6; k = 23.6, α95 = 2.9, K =31.3, A95 = 2.5; Fig.7, Table 1, Supplementary File SF1C). It demagnetizes between 240-560°C or 16-70 mT steps. Due to its consistency through sites and post-tilting character we have averaged all specimens (62) where we found it. The resulting component shares a common mean direction (Tauxe, 2010; Koymans et al., 2016) with the primary magnetization found in the neighbor El Viar Permian basin (named eP, for Early Permian, Fig. 7c.) (Weil et al., 2010). Hereafter we refer to this component as eP.

BD series show a shallow (between ~20º and -1º, Table 1), single polarity component with a varied E to SE trend (Between 95º and 125º; Fig. 8, Table 1). It unblocks from 240°C/16mT to full demagnetization. When occurring together with component eP, these samples usually contain a composite component that follows a great circle (especially in BD07, Fig. 8). This component clusters better between sites before any tilt correction, however, sites BD03 and BD04 cluster better after full tilt correction (Fig. 8, g and h). VGP distributions of this component are rounded in all sites, except for BD07, all passing the Deenen criteria

(Deenen et al., 2011) and with clustering (k) between 16.4 and 74 (Fig. 8 Table 1). Since this component is non uniformly rotated respect to eP, but show the same polarity and inclinations, we have denominated it "R" component (for Rotated). This component does not happen in BD08, which shows only eP component and BD02, whose 4 cores show a non compatible dec/inc = 13.8°/33.79°. Figure 8 and table 1 display the statistical parameters of BD series.

JaIb series show varied directions and results. JaIb1 shows a very elongated distribution that follows a great circle from present date field to a direction that was impossible to isolate, but that could resemble 'R' or 'eP' components (Fig. 9). Since we could not successfully isolate a direction from the distribution, we do not consider this site for interpretation or discussion. JaIb2 shows a shallow inclination, single polarity with declinations to the E that we consider the same as BD series' 'R' (Figure 9 and Table 1). In JaIb3 we could isolate both a present day (PD) and 'eP' components, which is the ChRM of this site.

In JaIb4 we could only retrieve a poorly clustered distribution around the SW quadrant of the stereonet in which clustering is only acceptable when we apply the 45˚ cut-off that arbitrary removes points that are visually part of the distribution. Inclinations and declinations are varied, from very shallow to very steep but always downwards, (Fig. 9 and Table 1). Finally, in JaIb5 we could identify a present day overprint (PD), as well as a set of scatter directions that we separated based on their magnetic mineralogy. All samples that unblock between 100°C and 350°C and 16-70 mT show a steep downwards average (Py component in Fig. 9 and Table 1). The rest of the directions show a really poor clustering (k = 5) with a possibly meaningless average around dec/inc=44.5/32.9 (Fig. 9 and Table 1). This is typically found between 100°C and 540°C and 12-60 mT. None of the latter pass a fold test (Supplementary file SF1-C). Due to the ambiguity, scattering and poor clustering of samples from the limestones of Ossa Morena we will exclude them from further interpretations.

The two sites of QM series gave insightful results with respect to previous studies. In QM01, we identified two components (Fig. 10). The first one is a well clustered single polarity, with moderately shallow inclinations and declinations to the ESE (Figure 10 and

Table 1). This component show the same declination and inclination to components "II" (Perroud et al., 1991) and "B" (Parés and van der Voo, 1992). It does not decay to the origin (Fig. 6) and demagnetizes between 200° to 520°C (thermal) and 20 to 60mT (AF) steps. We refer to this component as R_1. Due to the presence of pyrite that alters to magnetite over 400˚C, QM01 does not provide any interpretable results over 500˚C (e.g., Fig. 6, QM01-27). Nonetheless, we could identify a component that demagnetizes from 60 mT to full demagnetization in AF. In general only 3 or 4 steps are part of this component, in many cases with very low linearity, and Maximum Deviation Angles (MAD) over 15 (Fig. 6; Supplementary File SF5). We fitted it to mimic the procedure of previous studies in Almadén to fully compare all datasets (Supplementary file SF1C). However, previous authors include also thermal demagnetization in their interpretations despite the presence of sulfides. Our component shows poor clustering (k=5), shallow inclinations with a single polarity and declinations to the ENE (Fig. 10; Table 1). We named this component R_2, but cannot assure the reliability of this component and recommend caution in further usage.

In QM02, we identified a component that again shows single polarity, NE declinations and shallow inclinations. This component shows an elongated VGP in declination, in contrast to the expected at low latitudes, but still passes Deenen criteria (Deenen et al., 2011) (Fig. 10 and Table 1). The component was isolated between 200°C to 520°C and 12-50 mT (AF). After 520ºC there is a loss of linearity, which we attribute to the alteration. This component has a common true mean direction with R_2 of QM01 in geographic coordinates (Supplementary File SF1C) and does not pass a fold test (Fig. 10d). This component resembles the previously studied component "I" in the Silurian spilites and tuffs (our QM02; Perroud et al., 1991) and Component "C" Parés and van der Voo (1992) identified in the Devonian dolerite (our site QM01).

4 Significance of rock- and paleomagnetism

Thermomagnetic analysis and hysteresis loops show that the main magnetic carrier is (Ti-)magnetite in the majority of our sites from all BD, JaIb and QM series. We found hematite in some samples of BD01 and all of JaIb01 (Fig. 4). Thermomagnetic curves allowed us to identify the presence of pyrite in the BD06, JaIb4, JaIb5 and QM01. BD02, BD06 and JaIb5

shows a thermomagnetic curve that resembles greigite, especially due to the increase in magnetization after a 200ºC cycle (Dekkers et al., 2000; Fig. 4). BD06 and JaIb5 contains also pyrite. In the case of JaIb5, one of its paleomagnetic components is consistent with greigite or pyrrhotite (component "Py"). However, BD02 is a sedimentary Jasper, with a strong red coloration, which suggests a total oxidation in Fe3+. The samples from this site do not show decay corresponding to pyrrhotite, nor GRM effect in AF corresponding to Greigite. Therefore, we think that a magnetization carried by maghemite is the most reasonable interpretation.

4.1 Anisotropy of the Magnetic Susceptibility

AMS in the BD series show in general terms a composite compaction-tectonic AMS fabrics (Fig.6). In BD01 and BD03, k_{min} (roughly coincident with the pole to the bedding) and k_{int} are elongated towards each other defining a great circle (Fig.6). This setting suggests an early development of composite compaction-tectonic fabric. BD07 and BD08, with oblate shape and k_{min} perpendicular to the cleavage plane of the region (Trending to N110°) define a full tectonic AMS fabric. The close to vertical k_{max} may indicate little load during deformation which would facilitate upwards extension instead of orogen parallel.

JaIb series show mostly composites fabrics with a clear compaction element. In JaIb1, JaIb2, JaIb4 and JaIb5, k_{min} axis and k_{max} are parallel to bedding poles and the local fold axes respectively. JaIb3 (gabbro) shows an isotropic fabric indicating little deformation.

We interpret QM series' AMS as a tectonic fabric. In this case, k_{min} is perpendicular to D3 shear fragile-ductile foliation, which varies even between sites (Aller et al., 1986). We could not observe any relic of a putative compaction fabric in the spillite and tuff sequences.

4.2 Paleomagnetism

At the SW-most of Iberia we have identified three main components of magnetization: PD, eP and R. We interpret PD component as a viscous remanent magnetization, with the direction of the present day field in Iberia. Component eP (in BD01, BD03, BD06, BD07, BD08, JaIb2 and JaIb3)(Figure 7a) has a single polarity and very shallow inclinations,

which implies its acquisition occurred at a time when Iberia was located at equatorial latitude. It is coherent regionally, showing no differential rotations, clusters far better in geographic coordinates (Figure 7b, Table 1), and shares a common mean direction with primary early Permian magnetizations in Iberia (Figure 7c; Weil et al., 2019). We interpret eP as a post-orogenic, early Permian component acquired during the Kiaman reverse superchron (314 to 264 Ma, Langereis et al., 2010), at a time when western Iberia was a stable plate segment.

Component R_1 (QM01) shows very similar inclinations and declinations to the components described in previous studies (Perroud et al., 1991; Parés & Van der Voo, 1992). Due to the single polarity, shallow inclinations and CCW rotations, both previous studies attributed this component to a late Carboniferous remagnetization. Pastor-Galán et al. (2015b) re-interpreted this component as a syn-Cantabrian Orocline remagnetization since the rotations were coherent with the Cantabrian orocline but lesser than the expected. We support such interpretation.

We identified component R_2 in both Devonian dolerites and Silurian volcanics (QM01 and 02 respectively). Our interpretation of R_2 in QM01 (Devonian dolerite) is somewhat bold, using the poorly linear and weak last 3-4 steps. Parés and van der Voo (1992) identified a similar component with a linear fit of three thermal steps in the same outcrop (500˚, 550˚ and 600º C). Despite having much better thermal resolution (20˚C steps from 500˚C), we could not retrieve the component with thermal demagnetization, and instead got an alteration pattern (Fig. 6). Considering the presence of sulfides, we think that our AF data in QM01 is slightly more reliable than previous thermal demagnetization. Although it should be taken with care, our data in QM01 shows a common direction with R_2 in QM02. R_2 is also very similar to what Perroud et al. (1991) found in the Silurian Spillites before any correction. We found the same declination (62º) and the same inclinations in the sites they sampled previously. Perroud interpreted this component as Silurian in origin because of a potential better clustering after correcting for the eastern plunging axis of Almadén syncline. We sampled sites from the hinge and southern limb of the syncline where the axis is horizontal and tilt correction is straightforward, but R_2 does not pass a fold test (Fig. 10d). R_2 magnetization in Almadén is post-folding, and therefore post-Variscan D1 (post 340

Ma). We, therefore, consider R_1 and R_2 part of a general late Carboniferous rotated component, 'R' *sensu lato* (Fig. 11b).

Component R (s.l.) shows single polarity and shallow downwards inclinations, although slightly steeper than eP. We have corrected the tilt of BD03 and BD04 due to better clustering (Fig.7g), but especially to a far better inclination consistency. BD03 and BD04 inclinations before any tilt correction are too rotated to be post early Permian and too steep to be a post-variscan tilt magnetization (Pastor-Galán et al., 2016; Fig. 8h). Component R shows counter-clockwise (CCW) rotations of different magnitudes (from 20º in BD05 up to 70º in JaIb2) (Fig.11a) with respect to component eP. The rotation pattern implies differential vertical axis rotations within SW Iberia, which occurred during a protracted period of constant polarity, and prior to the magnetization of eP. In general terms we can define R as a post-deformation, shallow and single polarity magnetization that had to be acquired previously to 295 Ma (eP timing in Weil et al., 2013). This constrains R to ~314 to ~295 Ma acquisition, during Kiaman superchron.

5 Kinematic implications for the Variscan Belt

Timing of magnetization and counterclockwise rotations for Component R correspond to those observed elsewhere in the Cantabrian Orocline's southern limb (e.g. Pastor-Galán et al., 2011; 2015b; 2018). Structural and Paleomagnetic studies have shown that Western Iberia registered no major post-Variscan deformation and/or differential rotations events (e.g. Weil et al., 2019). Our eP component coincides with primary magnetization in the nearby El Viar basin and fits with the expected for stable Iberia during the Permian (Fig. 7; Weil et al., 2010). We used a Bootstrapped Orocline test applied to the Cantabrian zone (Pastor-Galán et al. 2017a; 2017b) to estimate the expected declination if our sites were part of the Cantabrian Orocline. The orocline test indicates the degree of differential vertical axis rotations underwent by differently striking orogenic segments. After plotting declination vs. strike, the best linear fit slope is 1 when all curvature is the result of orocline bending,and it is 0 if the curvature is not due to any vertical axis rotations (Schwartz and van der Voo 1983; Yonkee and Weil 2010; Pastor-Galán et al. 2017a). In the cases where the orocline test is well constrained on a multitude of datapoints, as the Cantabrian orocline test (Weil et

al. 2013), it is possible to infer the expected declination in a portion of the orocline knowing its strike. Following this procedure, we calculated reference declinations and uncertainties for all our sites assuming they were part of the southern limb of Cantabrian Orocline using the procedure of Pastor-Galán et al. (2017b). After that, we compared our R with both the expected declination and with our eP component, which marks the expected declination at the end of the rotations.

R components from sites BD01, 03, 04, 06, 07, JaIb2 together with R_2 (QM01 and 02) show rotations in agreement with the expected for such strike in the south limb of the Cantabrian Orocline (Fig. 12). R component in BD05 and R_1 in QM01 show less rotation than expected, and lie between such expected and the eP component. We interpret these components acquired their magnetization during the rotations that lead to Cantabrian Orocline formation. Therefore, they registered only a fraction of the rotation instead of the whole, in a similar fashion to the process described in Pastor-Galán et al. (2016; 2017b).

Our results show that the South Portuguese, Ossa Morena and the south Central Iberian zones rotated up to 90º CCW during the late Carboniferous-early Permian. At the South Portuguese Zone, rotations vary together with the strike of the orogen and with the same magnitude, implying differential vertical axis rotations and orocline bending (Fig. 10a; e.g. Schwartz and van der Voo 1983). Such result is in concordance with previous paleomagnetic studies to the north (Weil et al., 2013; Fernández-Lozano et al; 2016; Pastor-Galán et al., 2015b; 2016; 2017a; 2018), proving that most of Iberia, except the northernmost, comprise the southern limb of the Cantabrian Orocline (Fig. 2a). Altogether, paleomagnetic results from Iberia rule out a the Central Iberian curve as a coeval orocline to the south of the Cantabrian Orocline, which would require opposite sense (CW) late Carboniferous vertical axis rotations.

The sense and magnitude of the vertical axis rotations observed in SW Iberia imply that the Avalonian segment of Iberia (South Portuguese Zone) moved together with the southern limb of the Cantabrian Orocline. A reconstruction of the movement implied by paleomagnetism makes this unit parallel to the general trend of the Variscan orogen before the orocline bending. Such kinematic constraints discard the Laurussian rigid indenter into

Gondwana as the mechanism forming the Cantabrian Orocline (Simancas et al., 2013). This leaves the change in the stress field, from orogen perpendicular to orogen parallel compression, as the only plausible scenario to explain our present day datasets (e.g. Gutiérrez-Alonso et al., 2004; 2008a). At the same time, paleomagnetism from SW Iberia corroborates that the Cantabrian Orocline extended to both Gondwana and Laurrusia in its northern and southern limbs, confirming the Greater Cantabrian orocline hypothesis (Pastor-Galán et al., 2015a) (Fig.13).

Our results do not support significant sinistral movements in SW Iberia during the formation of the Cantabrian Orocline. Geochronological data from the sinistral shear zones (Dallmeyer & Quesada, 1994) indicate such movement happened previous to ~315 Ma, when our paleomagnetic constraints begin. Although kinematic evidence is still scarce, we think orogen parallel transport can successfully explain the formation of an early Carboniferous curved structure in Central Iberia and the left-lateral movements in SW Iberia. Structural data in the Central Iberian Zone suggest a D1 (early Carboniferous) origin for the Central Iberian curve (Pastor-Galán et al., 2019b; Azor et al., 2019; Dias da Silva et al. in press). Dias da Silva et al. (in press) defended that Galicia Tras-os-Montes is an early Carboniferous thin-skinned extrusion wedge that moved orogen-parallel. This movement would have formed the Central Iberian curve, possibly restricted to the surroundings of Galicia Tras-os-Montes Zone. In a similar fashion but at both margins scale, Murphy et al. (2016) suggested that an oblique or irregular collision between Gondwana and Laurrusia was responsible for early Carboniferous extrusion of different blocks in SW Iberia. This movement could explain the pre-Cantabrian Orocline left-lateral movements observed in SW Iberia.

Figure 13 sketches a simplified kinematic model for the evolution of the Greater Cantabrian Orocline that affected both Gondwana and Laurussia margins, from a roughly linear orogen (Fig. 13a) to its present shape (Fig. 13d). Following the available data (e.g. Weil et al., 2019) we suggest that the vertical axis rotation initiated between 315-310 Ma (Fig. 13a). With the protracted orogen-parallel shortening, the orogen began to buckle around a vertical axis. Dextral shear zones with some sinistral conjugates, shortening (especially at the core) and vertical axis rotations accomodated the deformation (Fig.13b). The magmatism that

accompanied the formation of the Cantabrian Orocline (Gutiérrez-Alonso et al., 2011; Pereira et al., 2014) caused pervasive remagnetizations which recorded intermediate-rotation directions, such as R_1 in Almadén, or BD05 in the South Portuguese Zone (Fig. 13c). At early Permian, the deformation can no longer be accommodated through vertical axis rotations (Weil et al., 2010; Pastor-Galán et al., 2011), forming crustal scale NE-SW faults (Fernández-Lozano et al., 2019).

The amount and quality of the kinematic observations indicating a secondary origin for the Greater Cantabrian Orocline are difficult to dispute. The Greater Cantabrian Orocline extended for at least ~1000km wide and ~2000km length limbs, through two continents and several major lithospheric scale structures. The Greater Cantabrian Orocline, including most Avalonia s.l. into it, surpasses all its traditional limits: the crustal scale shear zones in the Variscan hinterland (Weil et al., 2013, Gutiérrez-Alonso et al., 2016) and the Rheic Ocean suture (Ribeiro et al., 2007; Weil et al., 2010; Martínez Catalán, 2011). At the same time, the formation of the structure requires well over 1000 km of extension and shortening in a relatively short period of time. Structures accommodating convergence and extension, including large shear zones (like the Guadalquivir shear zone, in figure 13), crustal scale detachments and/or subduction zones are yet to be described. Potential areas accommodating shortening include the Picos de Europa (Merino-Tomé et al., 2009), Pyrenees and other areas in southern France or Italy (Pereira et al., 2014). Extension, however, is elusive. Sandovar et al., 2019 found that Atlantic conjugate margins of Iberia and Newfoundland were already extended at Triassic, before the extension leading the opening of the Atlantic. This is, perhaps, a plausible candidate place to have accommodated part of the extension.

Finding a mechanism causing the necessary far-field stress change to form such structure remains challenging. Most proposed models slightly modify previous plate reconstructions (Stampfli and Borel, 2002; Torsvik et al., 2012) relying on the basis of a smaller scale orocline (Gutiérrez-Alonso et al., 2004; 2008a; Johnston and Gutierrez-Alonso, 2010;Weil et al., 2010; Pastor-Galán et al., 2015b). The formation of a Greater Cantabrian Orocline questions not only the mechanisms proposed for its formation, but challenges the existing late Carboniferous plate reconstructions (e.g. Stampfli et al., 2013, Domeier and Torsvik,

2014). It also adds an interrogation to one of the main assumptions in plate tectonics, plate rigidity (Gordon, 1998, Torsvik et al., 2012).

6 Conclusions

- We found two magnetization events in SW Iberia, components eP and R. Component eP is a shallow single polarity component, coincident with early Permian pole of Iberia. We interpreted as an early Permian remagnetization. R is also a shallow, but less than eP, single polarity component. We interpreted it was acquired previously to eP but during the Kiaman superchron, with a prospective age of ca. 315-295 Ma. This component show between 30º and 70º counterclockwise rotations compared to eP component.
- Counterclockwise rotations are coeval and of the same magnitude to the observed in the southern limb of the Cantabrian Orocline. We support that all SW Iberia was part of the southern limb of the Cantabrian Orocline. Following this and previous results in Central Iberia, we conclude that the Central Iberian curve is not coeval nor genetically linked to the Cantabrian orocline.
- Kinematics of SW Iberia imply the South Portuguese Zone (of Laurrusian affinity) rotated together with the rest of the Cantabrian orocline. Therefore, we rule out a South Portuguse rigid-indenter as a buckling mechanism of the Cantabrian Orocline.
- The rotations involved in the formation of the Cantabrian Orocline trespassed the Rheic suture and several lithospheric scale structures both in its northern and southern limb confirming the hypothesis of a continental scale Greater Cantabrian Orocline.

Acknowledgments

We want to thank Icaro Frois Dias da Silva, Paulo Carlos, Saturnino Lorenzo Álvarez, André Torres and Fábio Marques,for their field assistance. BDLM, MJD, and WK are grateful for support by Utrecht University. This contribution is related to the ISES post doctoral grant to DPG (project no. WA.146101.2.656). DPG wants to thank David Robert Jones, a starman waiting in the sky, the one that blew his mind. The present work is a

contribution to IUGS-UNESCO's IGCP projects no. 574 "Bending and Bent Orogens, and Continental Ribbons", no. 597 "Amalgamation and Breakup of Pangaea" and no. 648 "Supercontinent Cycles & Global Geodynamics".

References

Aerden, D.G.A.M., 2004. Correlating deformation in Variscan NW-Iberia using porphyroblasts; implications for the Ibero-Armorican Arc. Journal of Structural Geology 26, 177–196. https://doi.org/10.1016/S0191-8141(03)00070-1

Aller, A., Bastida Ibáñez, J., Ortega Bernaldo de Quirós, Eduardo, F., Estaun, P., 1986. Aportación al conocimiento estructural del Sinclinal de Almadén. Boletín geológico y minero 97, 68–81.

Arenas, R., Díez Fernández, R., Rubio Pascual, F.J., Sánchez Martínez, S., Martín Parra, L.M., Matas, J., González del Tánago, J., Jiménez-Díaz, A., Fuenlabrada, J.M., Andonaegui, P., Garcia-Casco, A., 2016. The Galicia–Ossa-Morena Zone: Proposal for a new zone of the Iberian Massif. Variscan implications. Tectonophysics 681, 135–143. https://doi.org/10.1016/j.tecto.2016.02.030

Azor, A., Dias da Silva, Í., Gómez Barreiro, J., González-Clavijo, E., Martínez Catalán, J.R., Simancas, J.F., Martínez Poyatos, D., Pérez-Cáceres, I., González Lodeiro, F., Expósito, I., Casas, J.M., Clariana, P., García-Sansegundo, J., Margalef, A., 2019. Deformation and Structure, in: The Geology of Iberia: A Geodynamic Approach. pp. 307–348. https://doi.org/10.1007/978-3-030-10519-8_10

Borradaile, G.J., Jackson, M., 2004. Anisotropy of magnetic susceptibility (AMS): Magnetic petrofabrics of deformed rocks. Geological Society Special Publication. https://doi.org/10.1144/GSL.SP.2004.238.01.18

Calvín, P., Casas, A.M., Villalaín, J.J., Tierz, P., 2014. Reverse magnetic anomaly controlled by Permian igneous rocks in the Iberian Chain (N Spain). Geologica Acta 12, 193–207. https://doi.org/10.1344/GeologicaActa2014.12.3.2

Cambeses, A., Montero, P., Molina, J.F., Hyppolito, T., Bea, F., 2018. Constraints of mantle and crustal sources and interaction during orogenesis: A zircon SHRIMP U-Th-Pb and O isotope study of the 'calc-alkaline' Brovales pluton, Ossa-Morena Zone, Iberian Variscan Belt 661–683. https://doi.org/10.1016/j.lithos.2018.11.037

Deenen, M.H.L., Langereis, C.G., van Hinsbergen, D.J.J., Biggin, A.J., 2011. Geomagnetic secular variation and the statistics of palaeomagnetic directions. Geophysical Journal International 186, 509–520. https://doi.org/10.1111/j.1365-246X.2011.05050.x

Dekkers, M.J., Passier, H.F., Schoonen, M.A.A., 2000. Magnetic properties of hydrothermally synthesized greigite (Fe3S4)-II. High- and low-temperature characteristics. Geophysical Journal International 141, 809–819. https://doi.org/10.1046/j.1365-246X.2000.00129.x

Dias da Silva, Í., Pereira, M.F., Silva, J.B., Gama, C., 2018. Time-space distribution of silicic plutonism in a gneiss dome of the Iberian Variscan Belt: The Évora Massif (Ossa-Morena Zone, Portugal). Tectonophysics 747–748, 298–317. https://doi.org/10.1016/j.tecto.2018.10.015

Dias, R., Ribeiro, A., Romão, J., Coke, C., Moreira, N., 2016. A review of the arcuate structures in the Iberian Variscides; constraints and genetic models. Tectonophysics 681, 170–194. https://doi.org/10.1016/j.tecto.2016.04.011

Diez-Balda, M.A., 1995. Syn-collisional extensional collapse parallel to the erogenic trend in a domain of steep tectonics : the Salamanca Detachment Zone (Central Iherian Zone , Spain). Journal of Structural Geology 17, 163–182. https://doi.org/https://doi.org/10.1016/0191-8141(94)E0042-W

Domeier, M., 2016. A plate tectonic scenario for the Iapetus and Rheic oceans. Gondwana Research 36, 275–295. https://doi.org/10.1016/j.gr.2015.08.003

Domeier, M., Torsvik, T.H., 2014. Plate tectonics in the late Paleozoic. Geoscience Frontiers 5, 303–350. https://doi.org/10.1016/j.gsf.2014.01.002

Edel, J., Casini, L., Oggiano, G., Rossi, P., Schulmann, K., Cnrs, U.M.R., 2014. Early Permian 90º clockwise rotation of the Maures – Este Corsica – Sardinia block confirmed by new palaeomagnetic data and followed by a Triassic 60 8 clockwise rotation. Geological Society Special Publication 405, 333–361.

Eguiluz Alarcón, L., 1987. Petrogénesis de rocas ígneas y metamórficas en el antiforme Burguillo-Monesterio, macizo ibérico meridional. Universidad del País Vasco - Euskal Herriko Unibertsitatea.

Eldredge, S., Bachtadse, V., Van Der Voo, R., 1985. Paleomagnetism and the orocline hypothesis. Tectonophysics 119, 153–179. https://doi.org/10.1016/0040-1951(85)90037-X

Faure, M., Lardeaux, J., Ledru, P., 2009. A review of the pre-Permian geology of the Variscan French Massif Central. Comptes Rendus Geoscience 341, 202–213. https://doi.org/10.1016/j.crte.2008.12.001

Fernández-Lozano, J., Gutiérrez-Alonso, G., Willingshofer, E., Sokoutis, D., de Vicente, G., Cloetingh, S., 2019. Shaping of intraplate mountain patterns: The Cantabrian orocline legacy in Alpine Iberia. Lithosphere 11, 708–721. https://doi.org/10.1130/L1079.1

Fernández-lozano, J., Pastor-galán, D., Gutiérrez-alonso, G., Franco, P., 2016. Tectonophysics New kinematic constraints on the Cantabrian orocline : A paleomagnetic study from the Peñalba and Truchas synclines , NW Spain. Tectonophysics 681, 195–208. https://doi.org/10.1016/j.tecto.2016.02.019

Gonçalves, F., 1985. Contribuição para o conhecimento geológico do complexo vulcano-sedimentar de Toca da Moura (Alcácer do Sal). Serviços Geológicos de Portugal.

Gordon, R.G., 1998. THE PLATE TECTONIC APPROXIMATION: Plate Nonrigidity, Diffuse Plate Boundaries, and Global Plate Reconstructions. Annual Review of Earth and Planetary Sciences 26, 615–642. https://doi.org/10.1146/annurev.earth.26.1.615

Gutiérrez-Alonso, G., 1996. Strain partitioning in the footwall of the Somiedo Nappe: Structural evolution of the Narcea Tectonic Window, NW Spain. Journal of Structural Geology 18, 1217–1229. https://doi.org/10.1016/S0191-8141(96)00034-X

Gutiérrez-Alonso, G., Collins, A.S., Fernández-Suárez, J., Pastor-Galán, D., González-Clavijo, E., Jourdan, F., Weil, A.B., Johnston, S.T., 2015. Dating of lithospheric buckling: 40Ar/39Ar ages of syn-orocline strike-slip shear zones in northwestern Iberia. Tectonophysics 643, 44–54. https://doi.org/10.1016/j.tecto.2014.12.009

Gutiérrez-alonso, G., Fernández-suárez, J., 2004. Orocline triggered lithospheric delamination. Special Paper of the Geological Society of America 3. https://doi.org/10.1130/0-8137-2383-3(2004)383

Gutiérrez-Alonso, G., Fernández-Suárez, J., López-Carmona, A., Gärtner, A., 2018. Exhuming a cold case: The early granodiorites of the northwest Iberian Variscan belt-A Visean magmatic flare-up? Lithosphere 10. https://doi.org/10.1130/L706.1/4098555/l706.pdf

Gutíerrez-Alonso, G., Fernandez-Suarez, J., Weil, A.B., Murphy, J.B., Johnston, S.T., Nance, R.D., U, F.C., 2008. Self-subduction of the Pangaean global plate. Nature Geoscience 1, 549–553. https://doi.org/10.1038/ngeo250

Gutíerrez-Alonso, G., Johnston, S.T., Weil, A.B., Pastor-Galán, D., Fernandez-Suarez, J., 2012. Buckling an orogen : The Cantabrian Orocline. GSA Today 22, 4–9. https://doi.org/10.1130/GSATG141A.1.Figure

Gutiérrez-Alonso, G., Murphy, J.B., Fernández-Suárez, J., Hamilton, M.A., 2008. Rifting along the northern Gondwana margin and the evolution of the Rheic Ocean: A Devonian age for the El Castillo volcanic rocks (Salamanca, Central Iberian Zone). Tectonophysics 461, 157–165. https://doi.org/10.1016/j.tecto.2008.01.013

Gutiérrez-alonso, G., Murphy, J.B., Fernández-suárez, J., Weil, A.B., Franco, M.P., Gonzalo, J.C., 2011. Lithospheric delamination in the core of Pangea : Sm-Nd insights from the Iberian mantle. Geology 39, 155–158. https://doi.org/10.1130/G31468.1

Gutiérrez-Marco, J.C., Piçarra, J., Augusto, C., Meireles, P., Cózar, P., 2019. Early Ordovician-Devonian Passive Margin Stage in the Gondwanan Units of the Iberian Massif XXII. The Geology of Iberia: A Geodynamic Approach 2. https://doi.org/10.1007/978-3-030-10519-8_3

Hatcher, R., 2010. The Appalachian orogen: A brief summary, in: From Rodinia to Pangea: The Lithotectonic Record of the Appalachian Region.

Hirt, A.M., Lowrie, W., Clendenen, W.S., Kligfield, R., 1993. Correlation of strain and the anisotropy of magnetic susceptibility in the Onaping Formation: evidence for a near-circular origin of the Sudbury Basin. Tectonophysics 225, 231–254.

Izquierdo-Llavall, E., Roca, E., Xie, H., Pla, O., Muñoz, J.A., Rowan, M.G., Yuan, N., Huang, S., 2018. Influence of Overlapping décollements , Syntectonic Sedimentation , and Structural Inheritance in the Evolution of a Contractional System : The Central Kuqa Fold-and-Thrust Belt (Tian. Tectonics 2608–2632. https://doi.org/10.1029/2017TC004928

Jacques, D., Muchez, P., Sintubin, M., 2018a. Tectonophysics Superimposed folding and W-Sn vein-type mineralisation in the Central Iberian Zone associated with late-Variscan oroclinal buckling : A structural analysis from the Regoufe area (Portugal). Tectonophysics 742–743, 66–83. https://doi.org/10.1016/j.tecto.2018.05.021

Jacques, D., Vieira, R., Muchez, P., Sintubin, M., 2018b. Transpressional folding and associated cross-fold jointing controlling the geometry of post-orogenic vein-type W-Sn mineralization: examples from Minas da Panasqueira, Portugal. Mineralium Deposita 53, 171–194. https://doi.org/10.1007/s00126-017-0728-6

Johnston, S.T., Gutierrez-Alonso, G., 2010. The North American Cordillera and West European Variscides: Contrasting interpretations of similar mountain systems. Gondwana Research 17, 516–525. https://doi.org/10.1016/j.gr.2009.11.006

Johnston, S.T., Weil, A.B., Sciences, O., Csc, P.O.B.S.T.N., 2013. Oroclines : Thick and thin. Geological Society of America 643–663. https://doi.org/10.1130/B30765.1

Julivert, M., Fontboté, J., Ribeiro, A., Igme, L.C.-, Madrid, U., 1974, U., 1974. Memoria explicativa del mapa tectónico de la Península Ibérica y Baleares. Madrid.

Julivert, M., Marcos, A., 1973. Superimposed folding under flexural conditions in the Cantabrian Zone (Hercynian Cordillera, northwest Spain). American Journal of Science 273, 353–375. https://doi.org/10.2475/ajs.273.5.353

Kollmeier, J.M., Van Der Pluijm, B.A., Van Der Voo, R., 2000. Analysis of Variscan dynamics; early bending of the Cantabria-Asturias Arc, northern Spain. Earth and Planetary Science Letters 181, 203–216. https://doi.org/10.1016/S0012-821X(00)00203-X

Koymans, M.R., Langereis, C.G., Pastor-galán, D., Hinsbergen, D.J.J. Van, 2016. Computers & Geosciences Paleomagnetism . org : An online multi-platform open source environment for paleomagnetic data analysis. Computers and Geosciences 93, 127–137. https://doi.org/10.1016/j.cageo.2016.05.007

Langereis, G., Krijgsman, W., Muttoni, G., Menning, M., 2010. Magnetostratigraphy-concepts, definitions, and applications. Newsletters on Stratigraphy 43, 207–233. https://doi.org/10.1127/0078-0421/2010/0043-0207

Li, P., Rosenbaum, G., Donchak, P.J.T., 2012. Structural evolution of the Texas Orocline , eastern Australia. Gondwana Research 22, 279–289. https://doi.org/10.1016/j.gr.2011.09.009

Liñán, E., Quesada, C., Dallmeyer, R.D., Martinez-García, E., 1990. Ossa-Morena zone: rift phase (Cambrian), in: Pre-Mesozoic Geology of Iberia. pp. 259–66.

López-Carmona, A., Abati, J., Pitra, P., Lee, J.K.W., 2014. P – T – t constraints and geodynamic implications from blueschists and eclogites of the north Gondwanan margin in Iberia (Malpica – Tui complex , Galicia). Gondwana 15, North meets South, At Madrid 2–3. https://doi.org/10.13140/2.1.4048.0001

López-Moro, F.J., López-Plaza, M., Gutiérrez-Alonso, G., Fernández-Suárez, J., López-Carmona, A., Hofmann, M., Romer, R.L., 2018. Crustal melting and recycling: geochronology and sources of Variscan syn-kinematic anatectic granitoids of the Tormes Dome (Central Iberian Zone). A U–Pb LA-ICP-MS study. International Journal of Earth Sciences 107, 985–1004. https://doi.org/10.1007/s00531-017-1483-8

Lorenz, V., 1976. Formation of Hercynian subplates, possible causes and consequences. Nature 262, 374–377. https://doi.org/10.1038/262374a0

Lorenz, V., Nicholls, I.A., 1984. Plate and intraplate processes of Hercynian Europe during the late Paleozoic. Tectonophysics 107, 25–56.

LOTZE, F., 1945. Zur Gliederung der Varisziden der Iberischen Meseta. Geotekt. Forschg. 6, 78–92.

Mac Niocaill, C., 2000. A new Silurian palaeolatitude for eastern Avalonia and evidence for crustal rotations in the Avalonian margin of southwestern Ireland. Geophysical Journal International 141, 661–671. https://doi.org/10.1046/j.1365-246X.2000.00101.x

Marshak, S., 2004. Salients, Recesses, Arcs, Oroclines, and Syntaxes — A Review of Ideas Concerning the Formation of Map-view Curves in Fold-thrust Belts. AAPG Memoir 82, 131–156.

Martínez-Catalán, J., Rubio Pascual, F., Diez Montes, A., Diez-Fernandez, R., Gomez-Barreiro, J., Dias da Silva, Í.F., González-Clavijo, E., Ayarza, P., Alcock, J.E., 2014. The late Variscan HT / LP metamorphic event in NW and Central Iberia : relationships to crustal thickening , extension , orocline development and crustal evolution. Geological Society Special Publication 225–247.

Martínez-Catalán, J.R., 2012. The Central Iberian arc , an orocline centered in the Iberian Massif and some implications for the Variscan belt. International Journal of Earth Sciences 1299–1314. https://doi.org/10.1007/s00531-011-0715-6

Martínez-Catalán, J.R., 2011. Are the oroclines of the Variscan belt related to late Variscan strike-slip tectonics ? Terra Nova. https://doi.org/10.1111/j.1365-3121.2011.01005.x

Martínez-garcía, E., Martínez-garcía, E., 2013. An Alleghenian orocline : the Asturian Arc , northwestern Spain. International Geology Review 6814. https://doi.org/10.1080/00206814.2012.713544

McFadden, P., McElhinny, M., 1987. The combined analysis of remagnetization circles and direct observations in palaeomagnetism. Earth and Planetary Science Letters 87, 161–172.

Meijers, M.J.M., Smith, B., Pastor-Galán, D., Degenaar, R., Sadradze, N., Adamia, S., Sahakyan, L., Avagyan, A., Sosson, M., Rolland, Y., Langereis, C.G., Müller, C., 2017. Progressive orocline formation in the Eastern Pontides-Lesser Caucasus. Geological Society Special Publication 428, 117–143. https://doi.org/10.1144/SP428.8

Merino-Tomé, O.A., Bahamonde, J.R., Colmenero, J.R., Heredia, N., Villa, E., Farias, P., 2009. Emplacement of the Cuera and Picos de Europa imbricate system at the core of the Iberian-Armorican arc (Cantabrian zone, north Spain): New precisions concerning the timing of arc closure. Bulletin of the Geological Society of America 121, 729–751. https://doi.org/10.1130/B26366.1

Mullender, T.A.T., Frederichs, T., Hilgenfeldt, C., de Groot, L. V., Fabian, K., Dekkers, M.J., 2016. Automated paleomagnetic and rock magnetic data acquisition with an in-line horizontal "2G" system. Geochemistry, Geophysics, Geosystems 17, 3546–3559. https://doi.org/10.1002/2016GC006436

Mullender, T.A.T., Velzen, A.J. Van, Dekkers, M.J., 1993. Continuous drift correction and separate identification of ferrimagnetic and paramagnetic contributions in thermomagnetic runs. Geophysical Journal International 663–672.

Munhá, J., Oliveira, J., Ribeiro, A., Oliveira, V., Maleo, C.Q.-, 1986, U., 1986. Beja-Acebuches Ophiolite characterization and geodynamic significance. Maleo 2 13.

Munhá, J., Ribeiro, A., Fonseca, P., Oliveira, J.T., Castro, P., Quesada, C., 1989. Accreted terranes in Southern Iberia: Beja-Acebuches ophiolite and related oceanic sequences. 28th International Geological Congress, Washington DC (Vol. 20,.

Murphy, B.J., Braid, J.A., Quesada, C., Dahn, D., Gladney, E., Dupuis, N., 2016. An eastern Mediterranean analogue for the Late Palaeozoic evolution of the pangaean suture zone in SW Iberia. Geological Society Special Publication 424, 241–263. https://doi.org/10.1144/SP424.9

Nance, R.D., Gutiérrez-Alonso, G., Keppie, J.D., Linnemann, U., Murphy, J.B., Quesada, C., Strachan, R.A., Woodcock, N.H., 2010. Evolution of the Rheic Ocean. Gondwana Research 17, 194–222. https://doi.org/10.1016/j.gr.2009.08.001

O'Brien, T.M., van der Pluijm, B.A., 2012. Timing of Iapetus Ocean rifting from ar geochronology of pseudotachylytes in the St. Lawrence rift system of southern Quebec. Geology 40, 443–446. https://doi.org/10.1130/G32691.1

Oliveira, J.T., Quesada, C., Pereira, Z., Matos, J.X., Solá, A.R., Rosa, D., Albardeiro, L., Díez-Montes, A., Morais, I., Inverno, C., Rosa, C., Relvas, J., 2019. South Portuguese Terrane: A continental Affinity Exotic Unint, in: Geology of Iberia: A Geodynamic Approach. pp. 173–206. https://doi.org/10.1007/978-3-030-10519-8

Oliveria, J.T., González-Clavijo, E., Alonso, J., Aremandáriz, M., Bahamonde, J.R., Braid, J.A., Colmenero, J.R., Dias da Silva, Í., Fernandes, P., Fernández, L.P., Gabaldón, V., Jorge, R.S., Machado, G., Marcos, A., Merino-Tomé, Ó., Moreira, N., Murphy, J.B., Pinto de Jesus, A., Quesada, C., Rodrigues, B., Rosales, I., Sanz-López, J., Suárez, A., Villa, E., Piçarra, J.M., Pereira, Z., 2019. Synorogenic Basins, in: Geology of Iberia: A Geodynamic Approach. pp. 349–429.

Onézime, J., Charvet, J., Faure, M., Chauvet, A., Panis, D., 2002. Structural evolution of the southernmost segment of the West European variscides: The South Portuguese zone (SW Iberia). Journal of Structural Geology 24, 451–468. https://doi.org/10.1016/S0191-8141(01)00079-7

Opdike, N.D., Channel, J.E.T., 1996. Magnetic Stratigraphy, 64th ed. Internation Geophysics Series.

Palero-fernández, F.J., Martin-izard, A., Zarzalejos, M., Mansilla-plaza, L., 2014. Geological context and plumbotectonic evolution of the giant Almadén Mercury Deposit. Ore Geology Reviews 64, 71–88. https://doi.org/10.1016/j.oregeorev.2014.06.013

Parés, J.M., 2015. Sixty years of anisotropy of magnetic susceptibility in deformed sedimentary rocks. Frontiers in Earth Science 3, 1–13. https://doi.org/10.3389/feart.2015.00004

Parés, J.M., van der Voo, R., 1992. Paleozoic Paleomagnetism of Almaden , Spain : A Cautionary Note. Journal of Geophysical Research 97, 9353–9356.

Pastor-Galán, D., Dekkers, M.J., Gutiérrez-Alonso, G., Brouwer, D., Groenewegen, T., Krijgsman, W., Fernández-Lozano, J., Yenes, M., Álvarez-Lobato, F., 2016. Paleomagnetism of the Central Iberian curve's putative hinge: Too many oroclines in the Iberian Variscides. Gondwana Research. https://doi.org/10.1016/j.gr.2016.06.016

Pastor-Galán, D., Dias da Silva, Í.F., Groenewegen, T., Krijgsman, W., 2019. Tangled up in folds: tectonic significance of superimposed folding at the core of the Central Iberian curve (West Iberia). International Geology Review. https://doi.org/10.1080/00206814.2017.1422443

Pastor-Galán, D., Groenewegen, T., Brouwer, D., Krijgsman, W., Dekkers, M.J., 2015a. One or two oroclines in the Variscan orogen of Iberia? Implications for Pangea amalgamation. Geology. https://doi.org/10.1130/G36701.1

Pastor-Galán, D., Gutiérrez-alonso, G., Brandon, A., 2011. Tectonophysics Orocline timing through joint analysis : Insights from the Ibero-Armorican Arc. Tectonophysics 507, 31–46. https://doi.org/10.1016/j.tecto.2011.05.005

Pastor-Galán, D., Gutiérrez-Alonso, G., Meere, P.A., Mulchrone, K.F., 2009. Factors affecting finite strain estimation in low-grade, low-strain clastic rocks. Journal of Structural Geology 31, 1586–1596. https://doi.org/10.1016/j.jsg.2009.08.005

Pastor-Galán, D., Gutiérrez-Alonso, G., Zulauf, G., Zanella, F., 2012. Analogue modeling of lithospheric-scale orocline buckling: Constraints on the evolution of the Iberian-Armorican arc. Bulletin of the Geological Society of America 124, 1293–1309. https://doi.org/10.1130/B30640.1

Pastor-Galán, D., Langereis, C.G., Gutie, G., 2017a. Paleomagnetism in Extremadura (Central Iberian zone , Spain) Paleozoic rocks : extensive remagnetizations and further constraints on the extent of the Cantabrian orocline. Journal of Iberian Geology 43, 583–600. https://doi.org/10.1007/s41513-017-0039-x

Pastor-Galán, D., Martín-Merino, G., Corrochano, D., 2014. Tectonophysics Timing and structural evolution in the limb of an orocline : The Pisuerga – Carrión Unit (southern limb of the Cantabrian Orocline , NW Spain). Tectonophysics 622, 110–121. https://doi.org/10.1016/j.tecto.2014.03.004

Pastor-Galán, D., Mulchrone, K.F., Koymans, M.R., van Hinsbergen, D.J.J., Langereis, C.G., 2017b. Bootstrapped total least squares orocline test: A robust method to quantify vertical-axis rotation patterns in orogens, with examples from the Cantabrian and Aegean oroclines. Lithosphere 9, 499–511. https://doi.org/10.1130/L547.1

Pastor-Galán, D., Pueyo, E.L., Diederen, M., Garcia-Lasanta, C., Langereis, C.G., 2018. Late Paleozoic Iberian Orocline (s) and the Missing Shortening in the Core of Pangea . Paleomagnetism From the Iberian Range. Tectonics 37, 3877–3892. https://doi.org/10.1029/2018TC004978

Pastor-Galán, D., Ursem, B., Meere, P.A., Langereis, C., 2015b. Extending the Cantabrian Orocline to two continents (from Gondwana to Laurussia). Paleomagnetism from South Ireland. Earth and Planetary Science Letters 432, 223–231. https://doi.org/10.1016/j.epsl.2015.10.019

Pereira, M.F., Castro, A., Chichorro, M., Fernández, C., Díaz-Alvarado, J., Martí, J., Rodríguez, C., 2013. Chronological link between deep-seated processes in magma chambers and eruptions: Permo-Carboniferous magmatism in the core of Pangaea (Southern Pyrenees). Gondwana Research. https://doi.org/10.1016/j.gr.2013.03.009

Pereira, M.F., Castro, A., Fernández, C., 2015. The inception of a Paleotethyan magmatic arc in Iberia. Geoscience Frontiers 6, 297–306. https://doi.org/10.1016/j.gsf.2014.02.006

Pérez-Cáceres, I., Martínez Poyatos, D., Simancas, J.F., Azor, A., 2017. Testing the Avalonian affinity of the South Portuguese Zone and the Neoproterozoic evolution of SW Iberia through detrital zircon populations. Gondwana Research 42, 177–192. https://doi.org/10.1016/j.gr.2016.10.010

Pérez-Cáceres, I., Poyatos, D.M., Simancas, F., Azor, A., 2016. Testing the Avalonian affinity of the South Portuguese Zone and the Neoproterozoic evolution of SW Iberia through detrital zircon populations. Gondwana Research. https://doi.org/10.1016/j.gr.2016.10.010

Pérez-Cáceres, I., Martínez Poyatos, D., Simancas, J.F., Azor, A., 2015. The elusive nature of the Rheic Ocean suture in SW Iberia. Tectonics 34, 2429–2450. https://doi.org/10.1002/2015TC003947

Perroud, H., Bonhommet, M., Ribeiro, A., 1985. The Upper Devonian Beja Gabbro yields. Geophysical Rearch Letters 12, 45–48.

Perroud, H., Calza, F., Khattach, D., 1991. Paleomagnetism of the Silurian Volcanism at Almaden , Southern Spain. Journal of Geophysical Research 96, 1949–1962.

Pin, C., Fonseca, P.E., Paquette, J.L., Castro, P., Matte, P., 2008. The ca. 350 Ma Beja Igneous Complex: A record of transcurrent slab break-off in the Southern Iberia Variscan Belt? Tectonophysics 461, 356–377. https://doi.org/10.1016/j.tecto.2008.06.001

Pueyo, E.L., Pocoví, A., Parés, J.M., Millán, H., Larrasoana, J.C., 2003. Thrust ramp geometry and spurious rotations of paleomagnetic vectors. Studia Geophysica et Geodaetica 47, 331–357. https://doi.org/10.1023/A:1023775725268

Pueyo, E.L., Sussman, A.J., Oliva-Urcia, B., Cifelli, F., 2016. Palaeomagnetism in fold and thrust belts: Use with caution. Geological Society Special Publication 425, 259–276. https://doi.org/10.1144/SP425.14

Quesada, C., 1996. A reappraisal of the structure of the Spanish segment of the Iberian Pyrite Belt. Mineralium Deposita 31–44.

Quesada, C., Braid, J.A., Fernandes, P., Ferreira, P., Jorge, R.S., Matos, J.X., Murphy, J.B., Oliveira, J.T., Pedro, J., Pereira, Z., 2019. SW Iberia Variscan Suture Zone: Oceanic Affinity Units, in: The Geology of Iberia: A Geodynamic Approach. pp. 131–171. https://doi.org/10.1007/978-3-030-10519-8_5

Quesada, C., Dallmeyer, D.R., 1994. Tectonothermal evolution of the Badajoz-Cordóba shear zone (SW Iberia) : characteristics and 40Ar/39Ar mineral age constraints. Tectonophysics 231.

Ribeiro, A., Munhá, J., Dias, R., Mateus, A., Pereira, E., Ribeiro, L., Fonseca, P., Araújo, A., Oliveira, T., Romão, J., Chaminé, H., Coke, C., Pedro, J., 2007. Geodynamic evolution of the SW Europe Variscides. Tectonics 26, 1–24. https://doi.org/10.1029/2006TC002058

Ries, A.C., Shackleton, R.M., n.d. Patterns of Strain Variation in Arcuate Fold Belts. Philosophical Transactions of the Royal Society of London. Series A, Mathematical and Physical Sciences. https://doi.org/10.2307/74645

Robardet, M., Doré, F., 1988. The Late Orodovician Diamictitic Formations from Southwestern Europe: North-Gondwana glaciomarine deposits. Paleogeography 66, 19–31.

Rubio Pascual, F.J., López-Carmona, A., Arenas, R., 2016. Thickening vs. extension in the Variscan belt: P–T modelling in the Central Iberian autochthon. Tectonophysics 681, 144–158. https://doi.org/10.1016/j.tecto.2016.02.033

Sánchez-García, T., Chichorro, M., Solá, A.R., Álvaro, J.J., Díez-Montes, A., Bellido, F., Ribeiro, M.L., Quesada, C., Lopes, J.C., Dias da Silva, Í., González-Clavijo, E., Gómez Barreiro, J., López-Carmona, A., 2019. The Cambrian-Early Ordovician Rift Stage in the Gondwanan Units of the Iberian Massif, in: The Geology of Iberia: A Geodynamic Approach. pp. 27–74. https://doi.org/10.1007/978-3-030-10519-8_2

Sánchez-García, T., Bellido, F., Quesada, C., 2003. Geodynamic setting and geochemical signatures of Cambrian–Ordovician rift-related igneous rocks (Ossa-Morena Zone, SW Iberia). Tectonophysics 365, 233–255. https://doi.org/10.1016/S0040-1951(03)00024-6

Sandoval, L., Welford, J.K., Macmahon, H., Peace, A.L., 2019. Determining continuous basins across conjugate margins : The East Orphan , Porcupine , and Galicia Interior basins of the southern North Atlantic Ocean. Marine and Petroleum Geology 110, 138–161. https://doi.org/10.1016/j.marpetgeo.2019.06.047

Santos, J., Andrade, A., Portugal, J.M.-C.S.G., 1990, U., 1990. Magmatismo orogénico Varisco no limite meridional da Zona de Ossa-Morena. Comunicações de Serviços Geologicos, Porutgal.

Santos, J.F.H.P., Mata, J., Gonçalves, F., Munhá, J., 1987. Contribuição para o Conhecimento Geológico-Petrológico da Região de Santa Susana: O complexo Vulcano-Sedimentar da Toca da Moura. Comunicações de Serviços Geologicos, Porutgal 73, 29–48.

Schwartz, S.Y., Van der Voo, R., 1983. Paleomagnetic evaluation of the Orocline Hypothesis in the central and southern Appalachians. Geophysical Research Letters 10, 505–508. https://doi.org/10.1029/GL010i007p00505

Shaw, J., Johnston, S.T., 2016. Oroclinal buckling of the Armorican ribbon continent: An alternative tectonic model for Pangean amalgamation and Variscan orogenesis. Lithosphere 8, 769–777. https://doi.org/10.1130/L559.1

Shaw, J., Johnston, S.T., Gutiérrez-alonso, G., Weil, A.B., 2012. Oroclines of the Variscan orogen of Iberia: Paleocurrent analysis and paleogeographic implications. Earth and Planetary Science Letters 329–330, 60–70. https://doi.org/10.1016/j.epsl.2012.02.014

Simancas, J.F., Ayarza, P., Azor, A., Carbonell, R., Poyatos, D.M., Lodeiro, F.G., 2013. A seismic geotraverse across the Iberian Variscides: Orogenic shortening , collisional magmatism , and orocline development. Tectonics 32, 417–432. https://doi.org/10.1002/tect.20035

Simancas, J.F., Carbonell, R., González Lodeiro, F., Pérez Estaún, A., Juhlin, C., Ayarza, P., Kashubin, A., Azor, A., Martínez Poyatos, D., Sáez, R., Almodóvar, G.R., Pascual, E., Flecha, I., Martí, D., 2006. Transpressional collision tectonics and mantle plume dynamics: The Variscides of southwestern Iberia. Geological Society Memoir 32, 345–354. https://doi.org/10.1144/GSL.MEM.2006.032.01.21

Simancas, J.F., Tahiri, A., Azor, A., Martı, D.J., El, H., 2005. The tectonic frame of the Variscan – Alleghanian orogen in Southern Europe and Northern Africa. Tectonophysics 398, 181–198. https://doi.org/10.1016/j.tecto.2005.02.006

Stampfli, G.M., Borel, G.D., 2002. A plate tectonic model for the Paleozoic and Mesozoic constrained by dynamic plate boundaries and restored synthetic oceanic isochrons. Earth and Planetary Science Letters 196, 17–33. https://doi.org/10.1016/S0012-821X(01)00588-X

Stampfli, G.M., Hochard, C., Vérard, C., Wilhem, C., vonRaumer, J., 2013. The formation of Pangea. Tectonophysics. https://doi.org/10.1016/j.tecto.2013.02.037

Staub, R., 1927. Ideas sobre la tectónica de España. Córdoba.

Tait, J.A., Bachtadse, V., Soffel, H., 1996. Eastern Variscan fold belt: Paleomagnetic evidence for oroclinal bending. Geology 24, 871–874. https://doi.org/10.1130/0091-7613(1996)024<0871:EVFBPE>2.3.CO;2

Taylor, G.K., 2010. L. Tauxe 2010. Essentials of Paleomagnetism. , Geological Magazine. Cambridge University Press (CUP). https://doi.org/10.1017/s0016756810000555

Thomas, W.A., 1977. Evolution of Appalachain-Ouachita Salients and Recesses from Reentrants and Promontories in the continental margin. American Journal of Science 277, 1239–1278.

Torsvik, T., Cocks, L., 2016. Earth history and palaeogeography.

Torsvik, T.H., Voo, R. Van Der, Preeden, U., Mac, C., Steinberger, B., Doubrovine, P. V, Hinsbergen, D.J.J. Van, Domeier, M., Gaina, C., Tohver, E., Meert, J.G., Mccausland, P.J.A., Cocks, L.R.M., 2012. Earth-Science Reviews Phanerozoic polar wander , palaeogeography and dynamics. Earth Science Reviews 114, 325–368. https://doi.org/10.1016/j.earscirev.2012.06.007

Valladares, M.I., Barba, P., Ugidos, J.M., Colmenero, J.R., Armenteros, I., 2000. Upper Neoproterozoic ± Lower Cambrian sedimentary successions in the Central Iberian Zone (Spain): sequence stratigraphy , petrology and chemostratigraphy . Implications for other European zones. International Journal of Earth Sciences 2–20.

van der Boon, A., van Hinsbergen, D.J.J., Rezaeian, M., Gürer, D., Honarmand, M., Pastor-Galán, D., Krijgsman, W., Langereis, C.G., 2018. Quantifying Arabia–Eurasia convergence

accommodated in the Greater Caucasus by paleomagnetic reconstruction. Earth and Planetary Science Letters 482, 454–469. https://doi.org/10.1016/j.epsl.2017.11.025

van der Voo, R., 1969. Paleomagnetic evidence for the rotation of the Iberian Peninsula. Tectonophysics 7, 5–56. https://doi.org/10.1016/0040-1951(69)90063-8

Velzen, A.J., Zijderveld, J.D.A., 1995. Effects of weathering on single-domain magnetite in Early Pliocene marine marls. Geophysical Journal International 121, 267–278. https://doi.org/10.1111/j.1365-246X.1995.tb03526.x

Verges, J., 1983. Estudio del complejo volcano-sedimentario del devónico y de la estructura de la terminacion oriental del sinclinal de Almadén (Ciudad Real), in: Libro Jubilar J.M. Rios. pp. 215–229.

Weil, A., Gutiérrez-Alonso, G., Conan, J., 2010. New time constraints on lithospheric-scale oroclinal bending of the Ibero-Armorican Arc: A palaeomagnetic study of earliest Permian rocks from Iberia. Journal of the Geological Society 167, 127–143. https://doi.org/10.1144/0016-76492009-002

Weil, A., Pastor-Galán, D., Johnston, S.T., Gutiérrez-Alonso, G., 2019. Late/Post Variscan Orocline Formation and Widespread Magmatism, in: The Geology of Iberia: A Geodynamic Approach. pp. 527–542. https://doi.org/10.1007/978-3-030-10519-8_14

Weil, A.B., Gutiérrez-Alonso, G., Conan, J., 2019. New time constraints on lithospheric-scale oroclinal bending of the Ibero- Armorican Arc : a palaeomagnetic study of earliest Permian rocks from Iberia. Journal of the Geological Society 167, 127–143. https://doi.org/10.1144/0016-76492009-002.New

Weil, A.B., Gutiérrez-alonso, G., Johnston, S.T., Pastor-galán, D., 2013. Tectonophysics Kinematic constraints on buckling a lithospheric-scale orocline along the northern margin of Gondwana : A geologic synthesis. Tectonophysics 582, 25–49. https://doi.org/10.1016/j.tecto.2012.10.006

Weil, A.B., Sussman, A.J., 2004. Classifying curved orogens based on timing relationships between structural development and vertical-axis rotations. Geological Society of America Special Papers 3, 1–15. https://doi.org/10.1130/0-8137-2383-3(2004)383

Weil, A.B., van der Voo, R., Pluijm, B.A. Van Der, 2001. Oroclinal bending and evidence against the Pangea megashear : The Cantabria-Asturias arc (northern Spain). Geology November, 991–994.

Weil, A.B., Van Der Voo, R., Van Der Pluijm, B.A., Parés, J.M., 2000. The formation of an orocline by multiphase deformation: A paleomagnetic investigation of the Cantabria-Asturias Arc (northern Spain). Journal of Structural Geology 22, 735–756. https://doi.org/10.1016/S0191-8141(99)00188-1

Weil, A.B., Yonkee, A., 2009. Anisotropy of magnetic susceptibility in weakly deformed red beds from the Wyoming salient, Sevier thrust belt : Relations to layer-parallel shortening and orogenic curvature. Geological Society of America 235–256. https://doi.org/10.1130/L42.1

Yonkee, A., Weil, A.B., 2010. Reconstructing the kinematic evolution of curved mountain belts: Internal strain patterns in the Wyoming salient, Sevier thrust belt, U.S.A. Bulletin of the Geological Society of America 122, 24–49. https://doi.org/10.1130/B26484.1

Zjiderveld, J.D.A., 1967. A. C. Demagnetization of Rocks: Analysis of Results, in: Methods in Paleomagnetism. pp. 254–286. https://doi.org/10.1016/b978-1-4832-2894-5.50049-5

Captions

Fig. 1 - Simplified paleogeography of the winding Variscan-Alleghanian belt at pre-Pangea break-up times. In yellow, terranes with Gondwana affinity. In red tones, terranes with Laurussia affinity. Present day European Variscan outcrops are darker.(Modified after Martínez-Catalán et al., 2009).

Fig. 2 - A) Variscan zonation in Iberia and available Permo-Carboniferous paleomagnetic data.. e. (1) Weil et al., 2013 and references therein; (2) Fernandez-Lozano et al., 2016; (3) Pastor-Galán et al., 2018; (4) – Pastor Galán et al., 2016; (5) Osete et al., 1997; (6) Pastor-Galán et al., 2015b; (7) Pastor Galán et al., 2017; (8) Perroud et al., 1991 and Parés & Van der Voo, 1992; (9) Edel, 2014; (10) Weil et al., 2010; (11) Calvin et al., 2014 ; (12) Van der Voo et al., 1969; (13) Perroud et al., 1985. B - Simplified structure of the South Portuguese and Ossa-Morena zones and sampling sites C - Geological map of the Almadén syncline (Central Iberian Zone) with our sampling sites and those of Perroud et al. (1991), and Parés et al. (1992).

Fig. 3 - Kinematic sketch explaining the expected paleomagnetic data after: A) a collision of a rigid indenter, which would causes differential vertical in the indented block but not in the indenter B) An orocline bending/buckling involving two continental blocks, where all rotations have the same magnitude and are coeval.

Fig. 4 - Representative thermomagnetic curves and hysteresis loops of the different lithologies sampled. BD01-35 (spilites and Tuffs) show a magnetization drop at 580ºC, and hysteresis loop characteristic of hematite; BD02 (sedimentary Jasper) shows a maghemite thermomagnetic curve with pseudo-single domain loop; JaIb1 (wine-colored pillow lavas) show the main magnetic carrier is hematite, and an overcorrected hysteresis loop. JaIb3 shows a strong decay in magnetization between 540ºC characteristic of magnetite, with a near superparamagnetic hysteresis loop. QM01 (dolerite) shows the presence of pyrite oxidation effect starting at 420ºC, and a failed micromagnetic measurement.

Fig. 5 - Anisotropy of Magnetic Susceptibility results for South Portuguese Zone, Ossa-Morena Zone and Almadén Syncline. See text for details.

Fig. 6 - “Zjiderveld” diagrams and great circle fitting. Solid points represent projection in the horizontal plane, open points the vertical plane.

Fig. 7 - Component eP. (a) Virtual Geomagnetic Poles (VGP) and Equal area projection of all directions obtained for component eP. (b) Negative tilt test for all eP component (c) Positive common true mean direction test between our eP component and El Viar Permian basin primary magnetization (Weil et al., 2010).

Fig. 8 - (a) to (f) Virtual geomagnetic pole (VGP) projection (left) and equal area projection (right) of component R from the South Portuguese Zone. Grey circle in the VGP projections show the limit of a 45˚cutoff. (g) Positive tilt test for sites BD03 and BD04 (h) Tilt test for component R with BD03 and BD04 permanently corrected. It shows better clustering before tilt correction of the rest of BD series.

Fig. 9 - (a) to (f) Virtual geomagnetic pole (VGP) projection (left) and equal area projection (right) of components observed in the Ossa Morena Zone excluding eP and present day overprints (in Fig. 7 and SF1-C). Grey circle in the VGP projections shows the limit of a 45˚ cutoff.

Fig. 10 - (a) to (c) Virtual geomagnetic pole (VGP) projection (left) and equal area projection (right) of component R observed in the Almadén syncline. Grey circle in the VGP projections show the limit of a 45˚. (d) Negative fold test for component R_2.

Fig. 11 - (a) Declinations and parachute of confidence (ΔDec) of component R in the South Portuguese and Ossa-Morena Zones. Small red arrow shows the eP component declination.(b) Compilation of all paleomagnetic declination in the Almadén syncline. Green arrows indicate the pre-orocline directions of component R_2 (this study), II (Perroud et al., 1991) and C (Parés et al., 1992). Orange Arrows indicate syn-orocline formation components: R_1 (this study), B (Parés & Van der Voo., 1992) and I (Perroud et al., 1991).

Fig. 12 - Plot showing the observed paleomagnetic datasets for R component with their average declination and parachute of confidence (ΔDec, solid color); the eP parachute of confidence (empty and outlined in red); and the expected declination (empty parachute,

outlined in green), if each site rotated together the southern limb of the Cantabrian Orocline. We followed the procedure of Pastor Galán et al., (2017b).

Fig. 13 - Cartoon depicting the kinematic and paleomagnetic evolution of the Greater Cantabrian Orocline between ~310 and ~295 Ma. A) ca. 310 Ma - A roughly linear Variscan orogen (N-S in present day coordinates) showing all pre-orocline declinations. At this time Cantabrian Orocline begun to bend/buckle, perhaps due to a change in the stress field (e.g. Gutiérrez-Alonso et al., 2008). B) Ca. 307 - While the Cantabrian orocline buckled a series of major dextral and sinistral shear zones develop to accommodate part of this rotation (e.g. Gutiérrez-Alonso et al., 2016). Pervasive remagnetizations (orange arrows) occurred during the entire period (e.g. Pastor-Galán et al., 2017b), possibly due to the widespread magmatism in the Central Iberian Zone (e.g. Gutiérrez-Alonso et al., 2011) C) Ca. 303- The protracted buckling event also bent the shear zones. D) ca. 295 - Permian paleomagnetism indicates that no further vertical axis rotations occurred from this time (red arrows).

Table 1 - Statistics of paleomagnetic data. N Number of specimens that pass the cutoff. Ns number of specimens demagnetized, Dec - mean declination, Inc - mean inclination, k - precision parameter of directions, $\alpha 95$ - fisherian 95% confidence cone on directions, K - precision parameter of the poles, A95 - fisherian 95% confidence circle on poles, A95min and A95max describe the minimum and maximum values of A95 allowed to consider the average representative, λ - paleolatitude.

Supplementary Files

SF1 PDF document that contains extra information to help replicating results. A) Detailed site description and field photographs showing outcrop quality B) Supplemental rock magnetic analysis from every site with descriptions in each figure C) Supplemental figures about the components and fold-tests with their respective description.

SF2 Google Earth .kml file with the site locations.

SF3 Raw data files of our AMS and rock magnetism analyses. A) .ams files for Anisotropy of Magnetic Susceptibility. B) .hys files with data of micromagnetic data. C) .csv data with raw and results data for the thermomagnetic curves.

SF4 .col files for each site with the raw data and paleomagnetic interpretations. Files can be read with the open source and online paleomagnetism.org (v2.0 and onwards; Koymans et al., in press). These files contain the raw demagnetization data, our PCA fitting for each component identified in each site. The files also include lithology, bedding and site coordinates as metadata.

SF5 .pub files, that contain the interpreted components of each site and the statistical filters applied. Files can be opened with paleomagnetism.org (v2.0; Koymans et al., in press).

Supplementary Table 1 - Orogen strike measurements (with Von Mises uncertainty) and average of each site for application in the orocline test. Declinations calculated using the orocline test following Pastor-Galán et al. (2017b).

Supplementary Table 2 - Expected declination of each site, if part of the southern limb of the Cantabrian orocline, vs observed declination. The expected declination was calculated recurring to orogen trend measurements (fold axes strike) following Pastor-Galán et al. (2017b).

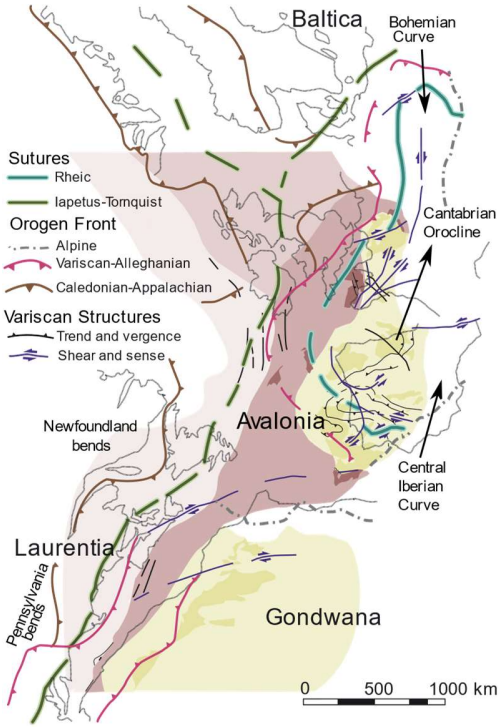
Baltica
Bohemian Curve
Sutures
Rheic
Iapetus-Tornquist
Orogen Front
Alpine
Variscan-Alleghanian
Caledonian-Appalachian
Variscan Structures
Trend and vergence
Shear and sense
Cantabrian Orocline
Newfoundland bends
Avalonia
Central Iberian Curve
Laurentia
Pennsylvania bends
Gondwana
0
500
1000 km

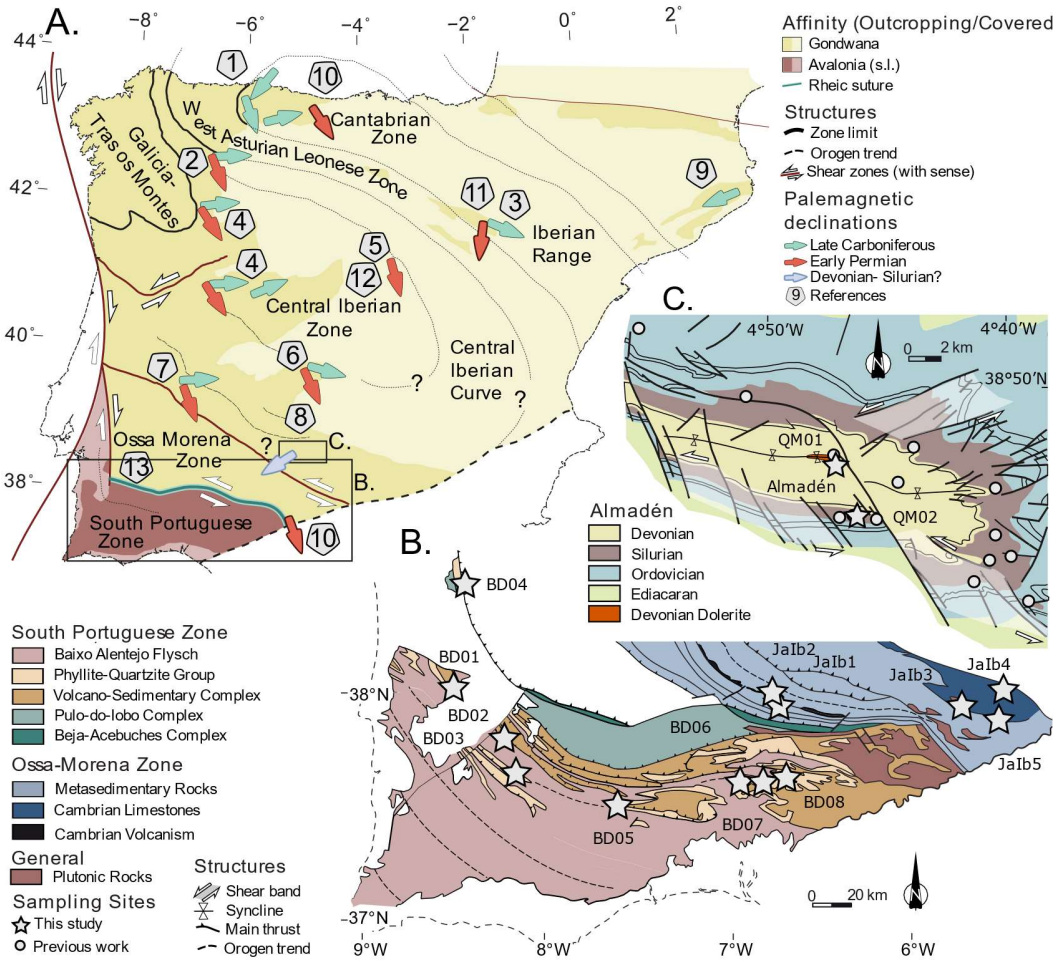
A.
B.
C.
Affinity (Outcropping/Covered
Gondwana
Avalonia (s.l.)
Rheic suture
Structures
Zone limit
Orogen trend
Shear zones (with sense)
Palemagnetic declinations
Late Carboniferous
Early Permian
Devonian- Silurian?
References
Cantabrian Zone
West Asturian Leonese Zone
Galicia-Tras os Montes
Iberian Range
Central Iberian Zone
Central Iberian Curve
Ossa Morena Zone
South Portuguese Zone
Almadén
Devonian
Silurian
Ordovician
Ediacaran
Devonian Dolerite
QM01
QM02
BD01
BD02
BD03
BD04
BD05
BD06
BD07
BD08
JaIb1
JaIb2
JaIb3
JaIb4
JaIb5
South Portuguese Zone
Baixo Alentejo Flysch
Phyllite-Quartzite Group
Volcano-Sedimentary Complex
Pulo-do-lobo Complex
Beja-Acebuches Complex
Ossa-Morena Zone
Metasedimentary Rocks
Cambrian Limestones
Cambrian Volcanism
General
Plutonic Rocks
Sampling Sites
This study
Previous work
Structures
Shear band
Syncline
Main thrust
Orogen trend

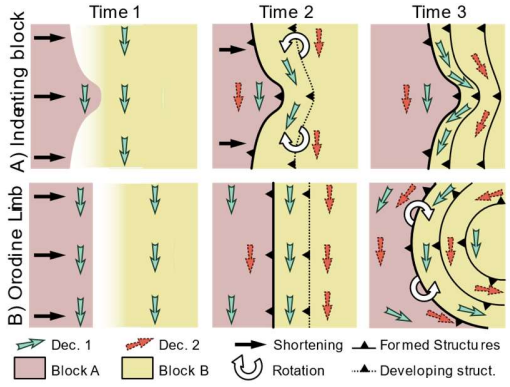
Time 1
Time 2
Time 3
A) Indenting block
B) Orodine Limb
Dec. 1
Dec. 2
Shortening
Formed Structures
Block A
Block B
Rotation
Developing struct.

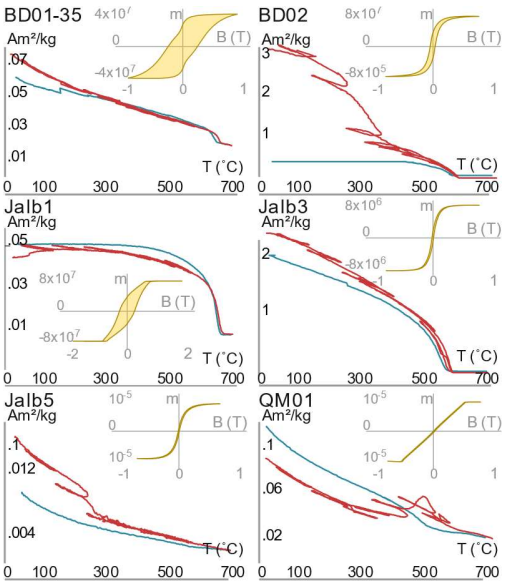
BD01-35
Am²/kg
.07
.05
.03
.01
T (°C)
0 100 300 500 700
BD02
Am²/kg
3
2
1
T (°C)
0 100 300 500 700
Jalb1
Am²/kg
.05
.03
.01
T (°C)
0 100 300 500 700
Jalb3
Am²/kg
2
1
T (°C)
0 100 300 500 700
Jalb5
Am²/kg
.1
.012
.004
T (°C)
0 100 300 500 700
QM01
Am²/kg
.1
.06
.02
T (°C)
0 100 300 500 700

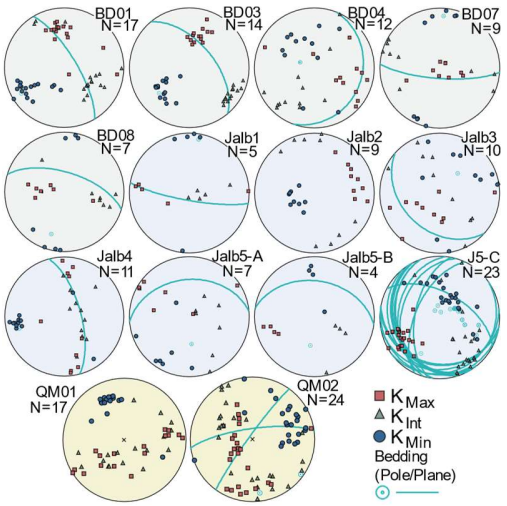
BD01 N=17
BD03 N=14
BD04 N=12
BD07 N=9
BD08 N=7
Jalb1 N=5
Jalb2 N=9
Jalb3 N=10
Jalb4 N=11
Jalb5-A N=7
Jalb5-B N=4
J5-C N=23
QM01 N=17
QM02 N=24
K Max
K Int
K Min
Bedding (Pole/Plane)

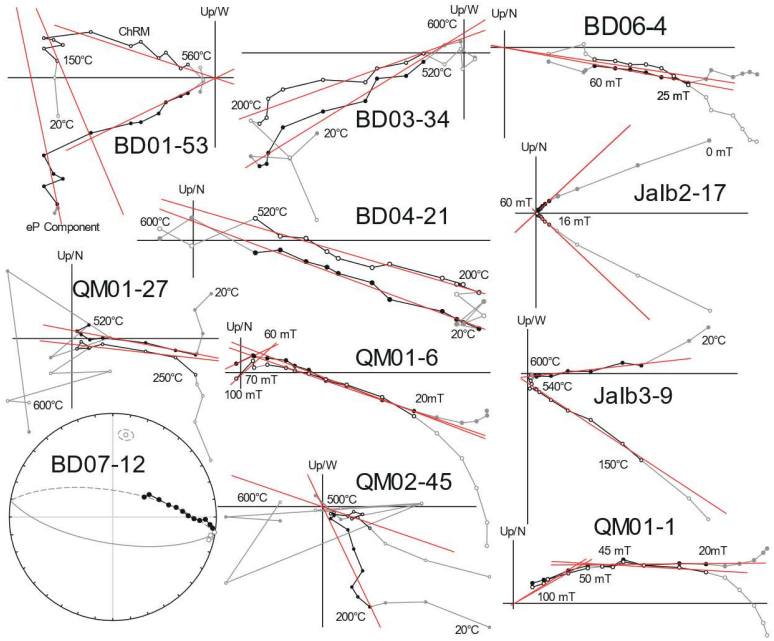
BD01-53
Up/W
ChRM
150°C
560°C
20°C
ePP Component
BD03-34
Up/W
600°C
520°C
200°C
20°C
BD06-4
Up/N
60 mT
25 mT
Jalb2-17
Up/N
0 mT
60 mT
16 mT
BD04-21
Up/N
600°C
520°C
200°C
20°C
QM01-27
Up/N
20°C
520°C
250°C
600°C
QM01-6
Up/N
60 mT
70 mT
100 mT
20mT
Jalb3-9
Up/W
20°C
600°C
540°C
150°C
BD07-12
QM02-45
Up/W
600°C
500°C
200°C
20°C
QM01-1
Up/N
45 mT
20mT
50 mT
100 mT

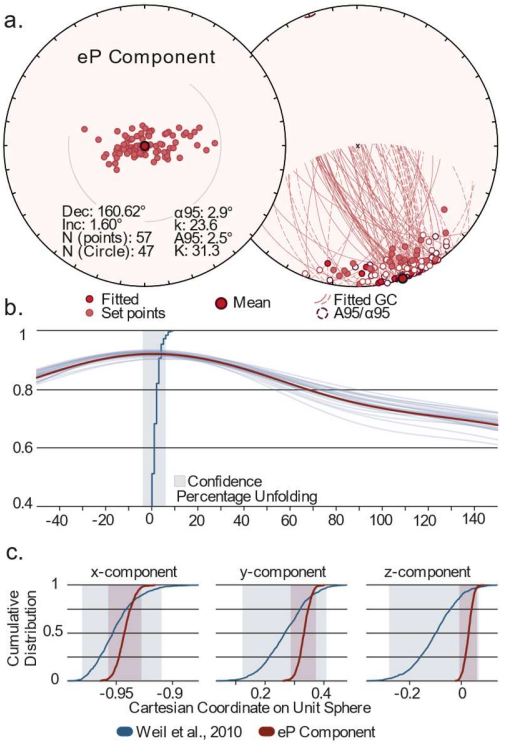
a.
ePP Component
Dec: 160.62°
Inc: 1.60°
N (points): 57
N (Circle): 47
α95: 2.9°
k: 23.6
A95: 2.5°
K: 31.3
b.
Fitted
Set points
Mean
Fitted GC
A95/α95
1
0.8
0.6
0.4
Confidence
Percentage Unfolding
-40
-20
0
20
40
60
80
100
120
140
c.
x-component
y-component
z-component
Cumulative Distribution
1
0.5
0
-0.95
-0.9
0.2
0.4
-0.2
0
Cartesian Coordinate on Unit Sphere
Weil et al., 2010
ePP Component

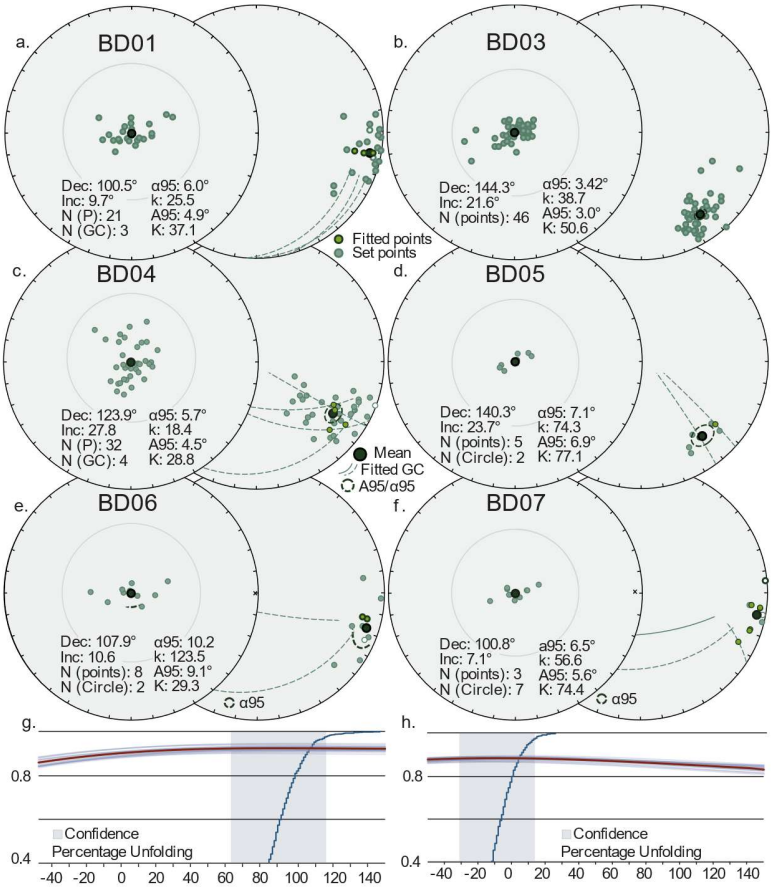
a.
BD01
Dec: 100.5°
Inc: 9.7°
N (P): 21
N (GC): 3
α95: 6.0°
k: 25.5
A95: 4.9°
K: 37.1
b.
BD03
Dec: 144.3°
Inc: 21.6°
N (points): 46
α95: 3.42°
k: 38.7
A95: 3.0°
K: 50.6
Fitted points
Set points
c.
BD04
Dec: 123.9°
Inc: 27.8
N (P): 32
N (GC): 4
α95: 5.7°
k: 18.4
A95: 4.5°
K: 28.8
d.
BD05
Dec: 140.3°
Inc: 23.7°
N (points): 5
N (Circle): 2
α95: 7.1°
k: 74.3
A95: 6.9°
K: 77.1
Mean
Fitted GC
A95/α95
e.
BD06
Dec: 107.9°
Inc: 10.6
N (points): 8
N (Circle): 2
α95: 10.2
k: 123.5
A95: 9.1°
K: 29.3
f.
BD07
Dec: 100.8°
Inc: 7.1°
N (points): 3
N (Circle): 7
α95: 6.5°
k: 56.6
A95: 5.6°
K: 74.4
α95
α95
g.
h.
0.8
0.4
Confidence
Percentage Unfolding
-40 -20 0 20 40 60 80 100 120 140

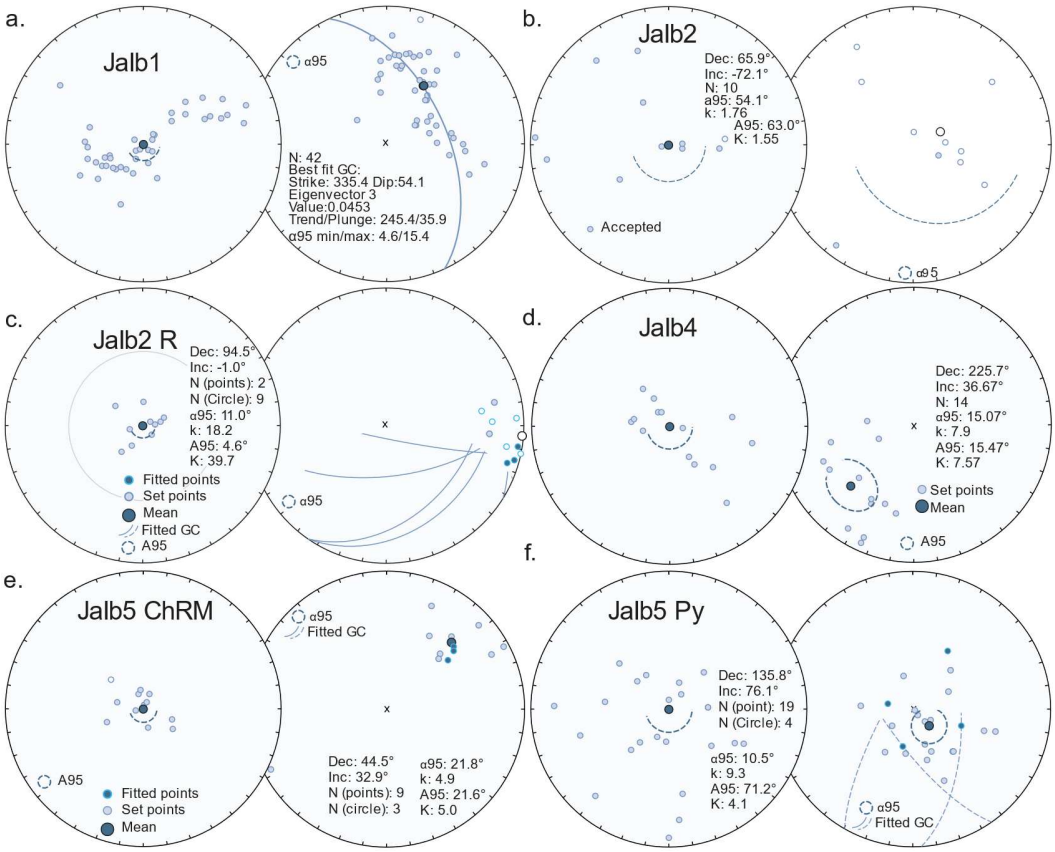
a.
Jalb1
α95
N: 42
Best fit GC:
Strike: 335.4 Dip:54.1
Eigenvector 3
Value:0.0453
Trend/Plunge: 245.4/35.9
α95 min/max: 4.6/15.4
b.
Jalb2
Dec: 65.9°
Inc: -72.1°
N: 10
a95: 54.1°
k: 1.76
A95: 63.0°
K: 1.55
Accepted
α95
c.
Jalb2 R
Dec: 94.5°
Inc: -1.0°
N (points): 2
N (Circle): 9
α95: 11.0°
k: 18.2
A95: 4.6°
K: 39.7
Fitted points
Set points
Mean
Fitted GC
A95
α95
d.
Jalb4
Dec: 225.7°
Inc: 36.67°
N: 14
α95: 15.07°
k: 7.9
A95: 15.47°
K: 7.57
Set points
Mean
A95
e.
Jalb5 ChRM
A95
Fitted points
Set points
Mean
α95
Fitted GC
Dec: 44.5°
Inc: 32.9°
N (points): 9
N (circle): 3
α95: 21.8°
k: 4.9
A95: 21.6°
K: 5.0
f.
Jalb5 Py
Dec: 135.8°
Inc: 76.1°
N (point): 19
N (Circle): 4
α95: 10.5°
k: 9.3
A95: 71.2°
K: 4.1
α95
Fitted GC

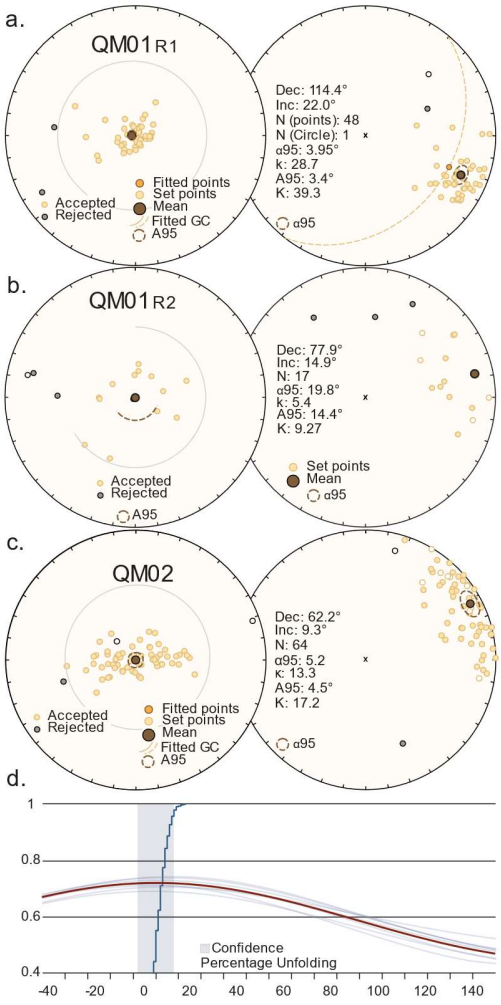
a.
QM01R1
Accepted
Rejected
Fitted points
Set points
Mean
Fitted GC
A95
Dec: 114.4°
Inc: 22.0°
N (points): 48
N (Circle): 1
α95: 3.95°
k: 28.7
A95: 3.4°
K: 39.3
α95
b.
QM01R2
Accepted
Rejected
A95
Dec: 77.9°
Inc: 14.9°
N: 17
α95: 19.8°
k: 5.4
A95: 14.4°
K: 9.27
Set points
Mean
α95
c.
QM02
Accepted
Rejected
Fitted points
Set points
Mean
Fitted GC
A95
Dec: 62.2°
Inc: 9.3°
N: 64
α95: 5.2
k: 13.3
A95: 4.5°
K: 17.2
α95
d.
1
0.8
0.6
0.4
Confidence
Percentage Unfolding
-40
-20
0
20
40
60
80
100
120
140

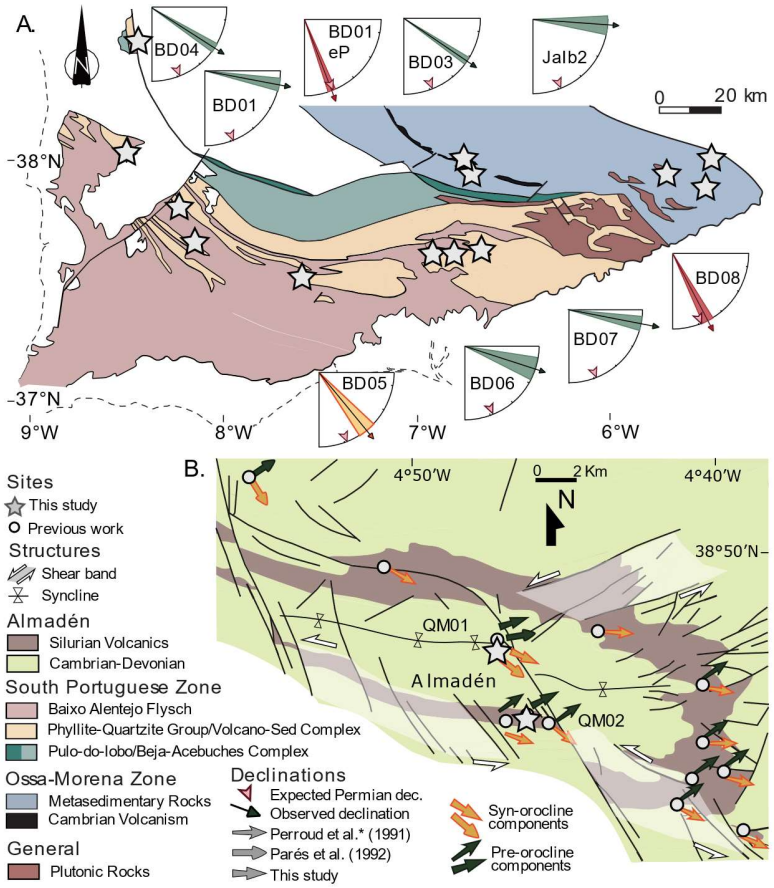
A.
BD04
BD01
eP
BD03
Jalb2
BD01
0 20 km
38°N
BD08
BD07
BD06
BD05
37°N
9°W
8°W
7°W
6°W
B.
4°50'W
0 2 Km
4°40'W
N
38°50'N
QM01
Almadén
QM02
Sites
This study
Previous work
Structures
Shear band
Syncline
Almadén
Silurian Volcanics
Cambrian-Devonian
South Portuguese Zone
Baixo Alentejo Flysch
Phyllite-Quartzite Group/Volcano-Sed Complex
Pulo-do-lobo/Beja-Acebuches Complex
Ossa-Morena Zone
Metasedimentary Rocks
Cambrian Volcanism
General
Plutonic Rocks
Declinations
Expected Permian dec.
Observed declination
Perroud et al.* (1991)
Parés et al. (1992)
This study
Syn-orocline components
Pre-orocline components

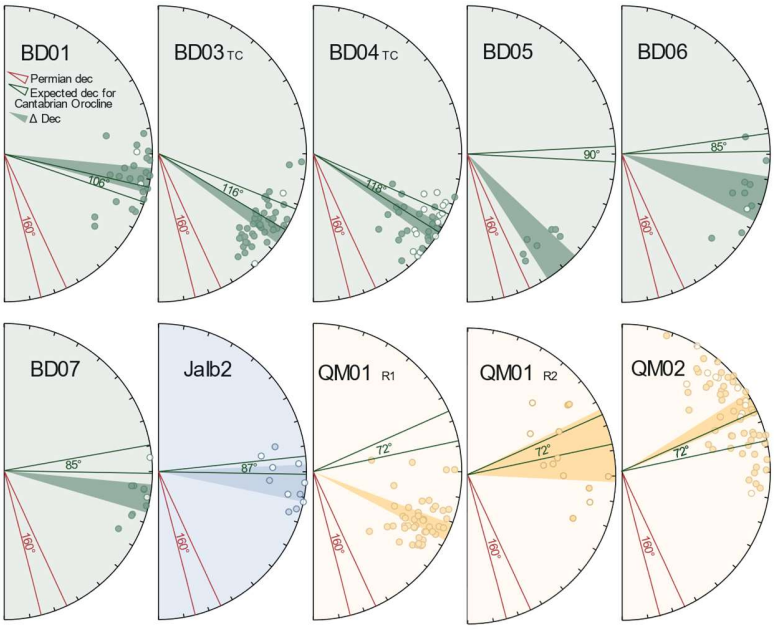
BD01
Permian dec
Expected dec for Cantabrian Orocline
Δ Dec
106°
160°
BD03 TC
116°
160°
BD04 TC
118°
160°
BD05
90°
160°
BD06
85°
160°
BD07
85°
160°
Jalb2
87°
160°
QM01 R1
72°
160°
QM01 R2
72°
160°
QM02
72°
160°

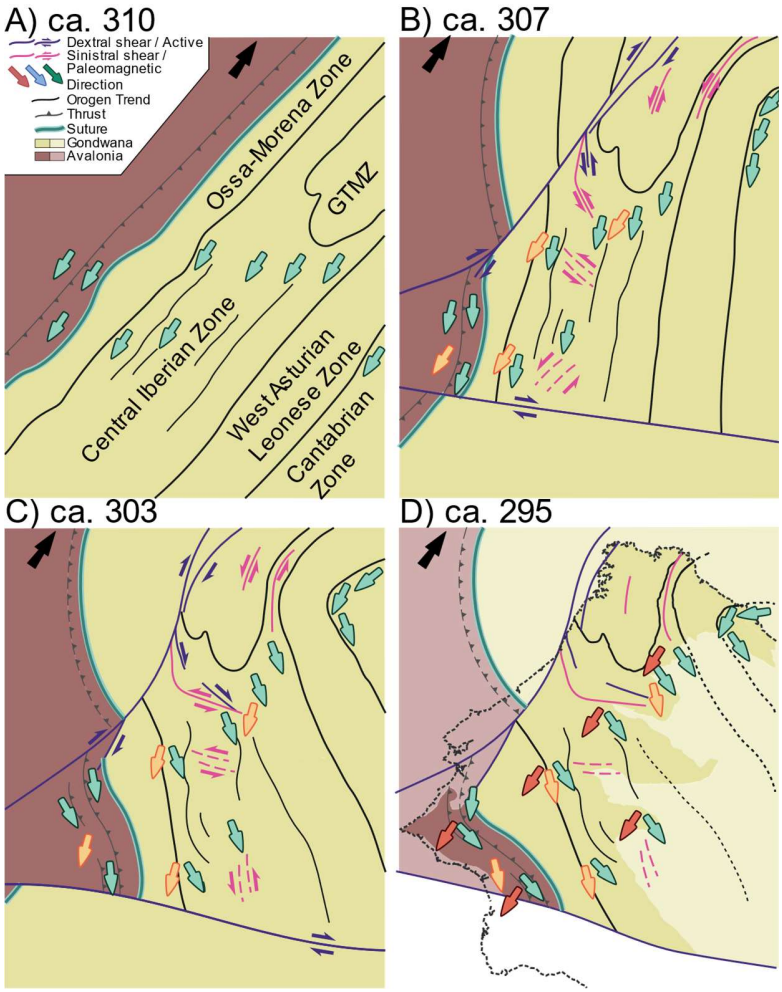
A) ca. 310
Dextral shear / Active
Sinistral shear /
Paleomagnetic
Direction
Orogen Trend
Thrust
Suture
Gondwana
Avalonia
Ossa-Morena Zone
GTMZ
Central Iberian Zone
West Asturian
Leonese Zone
Cantabrian
Zone
B) ca. 307
C) ca. 303
D) ca. 295